

1 Mechanisms of goethite dissolution in the presence of  
2 desferrioxamine B and Suwannee River fulvic acid at pH 6.5

3

4 Angela G. Stewart<sup>a, b</sup>, Karen A. Hudson-Edwards<sup>a</sup> and William E. Dubbin<sup>b\*</sup>

5

6

7

8 <sup>a</sup> Department of Earth and Planetary Sciences, Birkbeck, University of London,

9 Malet St., London WC1E 7X, UK

10 <sup>b</sup> Department of Earth Science, The Natural History Museum, Cromwell Road,

11 London SW7 5BD, UK. \*Corresponding author. Email: [b.dubbin@nhm.ac.uk](mailto:b.dubbin@nhm.ac.uk)

12 tel: +44 (0)20-7942-5616

13 fax: +44 (0)20-7942-5537

14

15

16

17

18

19

20 Abstract

21

22 Siderophores are  $\text{Fe}^{3+}$  specific low MW chelating ligands secreted by micro-  
23 organisms in response to Fe stress. Low MW organic acids such as oxalate have been shown  
24 to enhance siderophore mediated dissolution of  $\text{Fe}^{3+}$  oxides. However, the effect of fulvic  
25 acid presence on siderophore function remains unknown. We used batch dissolution  
26 experiments to investigate Fe release from goethite in the goethite-fulvic acid-  
27 desferrioxamine B (goethite-SRFA-DFOB) ternary system. Experiments were conducted at  
28 pH 6.5 while varying reagent addition sequence. FTIR and UV-Vis spectroscopy were  
29 employed to characterise the Fe-DFOB, Fe-SRFA and DFOB-SRFA complexes. Iron  
30 released from goethite in the presence of SRFA alone was below detection limit. In the  
31 presence of both SRFA and DFOB, dissolved Fe increased with reaction time, presence of the  
32 DFOB-SRFA complex, and where SRFA was introduced prior to DFOB. FTIR data show  
33 that in the ternary system,  $\text{Fe}^{3+}$  is complexed primarily to oxygen of the DFOB hydroxamate  
34 group, whilst the carboxylate C=O of SRFA forms an electrostatic association with the  
35 terminal  $\text{NH}_3^+$  of DFOB. We propose that SRFA sorbed to goethite lowers the net positive  
36 charge of the oxide surface, thus facilitating adsorption of cationic DFOB and subsequent  
37  $\text{Fe}^{3+}$  chelation and release. Furthermore, the sorbed SRFA weakens Fe-O bonds at the  
38 goethite surface, increasing the population of kinetically labile Fe. This work demonstrates  
39 the positive, though indirect role of SRFA in increasing the bioavailability of  $\text{Fe}^{3+}$ .

40

41

42

43 Keywords: siderophore, goethite, dissolution, Suwannee River fulvic acid,

44 desferrioxamine

## 1. INTRODUCTION

45  
46  
47  
48  
49  
50  
51  
52  
53  
54  
55  
56  
57  
58  
59  
60  
61  
62  
63  
64  
65  
66  
67  
68  
69

In oxic soils and sediments, Fe availability is limited by the low solubility of Fe oxides at circumneutral pH (Raymond and Dertz, 2004). To obtain Fe from these sparingly soluble phases, low MW Fe<sup>3+</sup>-chelating ligands known as siderophores are released by plants and micro-organisms (Haselwandter, 2008). For example, twice as much Fe is solubilised from goethite in the presence of 126 µM desferrioxamine B (DFOB), a trihydroxamate siderophore, than in the presence of 100 mM HCl at pH 3 over a 28-day reaction (Watteau and Berthelin, 1994). Furthermore, at hydroxamate siderophore concentrations typical of soils (i.e. 10<sup>-7</sup> – 10<sup>-8</sup> M; Powell et al., 1980), goethite solubility increases over a wide pH range (Kraemer, 2004), where the dissolution of goethite at pH > 4 is described as ligand-controlled (Holmén and Casey, 1996; Reichard et al., 2007a).

Iron(III) is coordinated to the hydroxamate groups of DFOB (Fig. 1) with Fe oxide dissolution influenced by siderophore concentration (Liermann et al., 2000), solution pH (Cervini-Silva, 2008) and temperature (Cocozza et al., 2002). As revealed by single-crystal X-ray diffraction, the chelate molecule consists of two closed loops and a free chain containing a protonated amine (Dhungana et al, 2001). The six hydroxamate oxygen atoms coordinate Fe<sup>3+</sup> and form a distorted octahedral geometry around the metallic centre (Cozar et al., 2006; Domagal-Goldman et al., 2009) (Fig. 1b). As a consequence of this complexation, the hydroxamate (oxime) protons are lost and the goethite hydroxyl or water groups coordinating Fe<sup>3+</sup> are displaced.

Iron release from goethite may be enhanced by the presence of low MW organic acids. For example, goethite dissolution by 5 × 10<sup>-5</sup> M oxalate, malonate or succinate at pH 6 yielded 10<sup>-11</sup> M Fe following 400 h reaction (Reichard et al., 2007a) while the presence of citrate produced 10<sup>-7</sup> M Fe and fumarate yielded undetectable levels of dissolved Fe. When

70 DFOB was added to those systems containing both goethite and low MW organic acids,  
71 greater amounts of Fe were released than in DFOB-only goethite systems. For example,  
72 soluble Fe concentrations increased from  $10^{-11}$  M to  $10^{-5}$  M when  $5.0 \times 10^{-5}$  M DFOB was  
73 added to a goethite suspension along with equimolar concentrations of the organic ligands  
74 listed above, except for citrate, for which soluble Fe increased only marginally, from  $10^{-7}$  M  
75 to  $10^{-6}$  M.

76 Fulvic acid (FA) (Fig. 2), the acid soluble component of humic substances are, along  
77 with hydrous Fe oxides and siderophores, ubiquitous in soils and sediments (Stevenson,  
78 1985). Fulvic acid sorbs strongly to goethite surfaces at pH values below the point of zero  
79 charge for goethite (i.e.  $< 9.2$ , Filius et al., 2000). This adsorption involves the formation of  
80 inner-sphere complexes via ligand exchange between the oxygen of FA carboxylate groups  
81 and the surface oxygen atoms coordinated to Fe at the goethite surface (Filius et al., 2003).  
82 Fourier transform infrared (FTIR) spectroscopy confirms the formation of this inner-sphere  
83 Fe-fulvate complex by virtue of a shift in the asymmetric carboxylate stretch vibration at pH  
84 5 (Fu and Quan, 2006). Humic compounds obtained from various natural environments also  
85 complex strongly, and reversibly, with mononuclear Fe, exhibiting stability constants of  
86  $10^{21.0}$  to  $10^{21.4}$  for Fe-humic complexes isolated from a river plume (Muller and Batchelli,  
87 2011), with lower stability constants (i.e.  $K = 10^{11.5}$  to  $10^{14.0}$ ) observed for Fe-FA complexes  
88 obtained from soil (Pandeya, 1993).

89 Although the effects of low MW acids such as oxalate and citrate on DFOB mediated  
90 dissolution of goethite have been examined previously (Reichard et al., 2007a,b), the  
91 influence of the higher MW fulvic acid has not yet been explored despite the ubiquity of this  
92 humic material in soils and sediments. In this paper we report, for the first time, the results of  
93 batch experiments examining the dissolution of goethite in the presence of both Suwannee  
94 River fulvic acid (SRFA) and DFOB. The effects of SRFA presence and reagent addition

95 sequence were investigated at pH 6.5 to elucidate dissolution mechanisms. The aims of the  
96 study were to: (i) determine the effect of SRFA presence on goethite dissolution by DFOB;  
97 (ii) develop a mechanistic model of how SRFA influences DFOB function; (iii) characterise  
98 possible aqueous Fe-DFOB and Fe-SRFA complexes formed; (iv) propose an overall  
99 dissolution mechanism for the goethite-DFOB-SRFA system.

100

101

## 2. MATERIALS AND METHODS

102

### 2.1. Goethite synthesis and characterisation

104

105 Goethite was synthesised following the method of Schwertmann and Cornell (1991).  
106 Briefly, 180 mL of 5 M KOH (Fisher Chemicals, SLR) was rapidly added to 100 mL of 1 M  
107  $\text{Fe}(\text{NO}_3)_3 \cdot 9\text{H}_2\text{O}$  (BDH, AnalaR) in a 2 L plastic beaker with constant stirring for 10 min. The  
108 suspension was brought to 2 L with ultrapure water (18 M $\Omega$ -cm, Milli-Q Millipore) and  
109 transferred to five 500 mL amber wide-mouth Nalgene HDPE screw top bottles then aged for  
110 24 h at 70 °C (Dubbin and Ander, 2003). The precipitate was washed with ultrapure water  
111 through a Büchner funnel into a Büchner flask using Whatman no. 40 filter paper, which was  
112 replaced after every 250 mL of suspension to prevent clogging. The precipitate was then  
113 allowed to air-dry at 21 °C.

114 The hydroxy Fe precipitates were confirmed as goethite ( $\alpha$ -FeOOH) by powder X-ray  
115 diffraction (XRD) analyses on an Enraf-Nonius PSD 120, equipped with an INEL 120°  
116 curved position sensitive detector utilising Cu K $\alpha_1$  radiation (45 kV and 45 mV) at 25 °C. N<sub>2</sub>  
117 multipoint BET surface area measurements were carried out using a Micrometrics Gemini III  
118 2375 instrument. Samples were allowed to de-gas with N<sub>2</sub> at 100 °C for 24 h prior to surface

119 area determination. A kaolinite standard ( $15.9 \pm 0.8 \text{ m}^2/\text{g}$ ) was analysed alongside the  
120 goethite samples to monitor accuracy.

121

## 122 2.2. Batch dissolution experiments

123

124 Stock solutions of: (i) DFOB obtained as the mesylate salt  
125  $[(\text{C}_{25}\text{H}_{46}\text{N}_5\text{O}_8\text{NH}_3^+(\text{CH}_3\text{SO}_3^-))$ , MW  $656 \text{ g mol}^{-1}$ ] (Sigma-Aldrich); (ii) SRFA purchased from  
126 the International Humic Substance Society [IHSS, Sample 1S101F, MW  $1360 \text{ g mol}^{-1}$  (Chin  
127 et al., 1994)]; and (iii) synthetic goethite ( $\alpha\text{-FeOOH}$ ) were prepared in a combined  
128 buffer/electrolyte (MOPS/ $\text{NaNO}_3$ ) solution for subsequent use in the batch dissolution  
129 experiments. Both DFOB and SRFA were used as received to prepare a  $500 \mu\text{M}$  stock  
130 solution of DFOB ( $0.823 \text{ g}$  DFOB dissolved in  $250 \text{ mL}$  MOPS/ $\text{NaNO}_3$  solution) and a  $65 \text{ mg}$   
131  $\text{C L}^{-1}$  stock solution of SRFA ( $0.0624 \text{ g}$  SRFA dissolved in  $500 \text{ mL}$  MOPS/ $\text{NaNO}_3$  solution).  
132 The goethite stock suspension was prepared to a concentration of  $1256 \text{ mg L}^{-1}$  ( $3.14 \text{ g}$   
133 goethite in  $2500 \text{ mL}$  MOPS/ $\text{NaNO}_3$  solution). The combined MOPS/ $\text{NaNO}_3$  solution  
134 consisted of  $1 \text{ mM}$  3-(N-morpholino) propanesulfonic acid (MOPS), a non-complexing  
135 buffer (Electran VWR BDH PRO LAB molecular biology grade; pH range  $6.5 - 7.9$ ;  $\text{pK}_a$   
136  $7.2$ ), and  $10 \text{ mM}$   $\text{NaNO}_3$  (BDH AnalaR). The pH of the MOPS/ $\text{NaNO}_3$  solution was  
137 increased from pH  $4.5$  to  $6.5$  with the drop-wise addition of  $0.1 \text{ M}$  NaOH (BDH ARISTAR),  
138 continuously monitored with a HANNA Instruments pH meter calibrated at two points (pH  
139  $4.01$  and  $7.01$ ). The pH of the goethite suspensions, and DFOB and SRFA solutions, were  
140 within the required range therefore no adjustment was required. Solutions and suspensions  
141 were stored in amber HDPE wide-mouth screw top bottles to protect from photo-induced  
142 reactions and stored at  $4 \text{ }^\circ\text{C}$  to restrict microbial growth. All glassware and plasticware was

143 washed thoroughly with phosphate-free detergent (Decon 90) then rinsed several times with  
144 ultra pure water.

145 Fig. 3 shows the reagents, addition sequences, and reaction times for each of the ten  
146 batch experiments. For batch experiments 1 through 8 (carried out in duplicate) 90 mL of  
147 goethite suspension was dispensed into each of eight 250 mL amber HDPE bottles. One of  
148 these eight bottles contained goethite alone (system 8), while a further two bottles without  
149 goethite served as procedural blanks to check for adsorption of DFOB (system 9) and SRFA  
150 (system 10) onto container walls. Subsequently, 9 mL of DFOB stock solution or 30 mL of  
151 SRFA stock solution were added to the bottles (with the exception of systems 3 and 5) as  
152 indicated in Fig. 3. The DFOB-SRFA complex was equilibrated for 30 minutes before  
153 addition to the goethite suspension (system 6). All batches were brought to a total volume of  
154 129 mL with MOPS/NaNO<sub>3</sub> and left to equilibrate for 24 h at 25 °C on an orbital shaker  
155 (Orbital Incubator SI50) at 100 rpm.

156 Following the initial 24 h contact, further reagents were added as indicated in Fig. 3,  
157 brought to final volumes of 168 mL, then placed on the orbital shaker for the duration of the  
158 reaction. In systems 3 and 5 we added DFOB and SRFA 4 h before the subsequent addition  
159 of, respectively, SRFA and DFOB, to more fully explore the effect of DFOB and SRFA  
160 addition sequence. A 4 hour reaction time was chosen because this duration had been  
161 reported as the optimal reaction period to achieve ligand adsorption without significant  
162 dissolution (Cocozza et al., 2002). The concentration of DFOB, where present, was 270 μM  
163 in all batch experiments. The pH of the suspensions in the 250 mL bottles was measured  
164 before and after the initial 24 h period, and at the end of the 330 h reaction. In all cases the  
165 pH was maintained at 6.5 and did not need further adjusting. Maintaining pH at 6.5 ensured  
166 that proton promoted dissolution was negligible. Changes in H<sup>+</sup> activity may also influence  
167 ligand-controlled goethite dissolution by modifying the concentrations and speciation of

168 adsorbed ligands (Reichard et al., 2007b). Subsamples of the suspensions were obtained at  
169 intervals throughout the 330 h reaction, then filtered through 25 mm cellulose acetate filters  
170 (pore size 0.2  $\mu\text{m}$ ) followed by filtration through 25 mm nitrocellulose membrane filters  
171 (pore size 0.025  $\mu\text{m}$ ) into clear polythene screw cap tubes.

172

### 173 2.3. Analysis of supernatant solutions

174

175 Five mL portions of the filtrates were acidified with 100  $\mu\text{L}$  70%  $\text{HNO}_3$  (Fisher  
176 Scientific) to prevent precipitation of Fe hydroxide then stored at 4  $^\circ\text{C}$ . These solutions were  
177 analysed for Fe using inductively coupled plasma atomic emission spectroscopy (ICP-AES)  
178 analysis (VARIAN VISTA PRO Program ICP Expert version 4.1.0; emission line 259.94 nm;  
179 detection limit 89 nmol  $\text{Fe L}^{-1}$ ). Aqueous SRFA and DFOB were quantified by UV-Vis  
180 spectroscopy (section 2.5). Total aqueous organic carbon (TOC) was determined by wet  
181 combustion with a Shimadzu 5000 TOC analyser after acidification of the filtrate with 10  $\mu\text{L}$   
182 concentrated HCl (BDH ARISTAR). To test the reliability of SRFA quantification by UV-  
183 Vis spectroscopy (Gan et al., 2007; Ghabbour and Davies, 2009), aqueous SRFA  
184 concentrations were also determined by TOC analysis, subtracting from the total organic C,  
185 that C assigned to DFOB as determined by chelometric UV-Vis spectroscopy analysis  
186 (section 2.5). Statistical significance among aqueous Fe, DFOB and SRFA concentrations for  
187 all batches was determined by applying the unpaired two-tailed Student's *t*-test with a level of  
188 significance of  $p = 0.05$ . The precipitate retained on each membrane filter following filtration  
189 was air-dried at room temperature, placed in an air tight container and preserved for  
190 subsequent observation by scanning electron microscopy (SEM), atomic force microscopy  
191 (AFM) and FTIR analysis, described below.

192



## 193 2.4. FTIR spectroscopy

194

195 Synthetic goethite, untreated SRFA and DFOB, and aqueous complexes of SRFA and  
196 DFOB prepared in several mole ratios (2:1 Fe<sup>3+</sup>-DFOB, 5:1 Fe<sup>3+</sup>-SRFA, 1:1 DFOB-SRFA,  
197 and 5:1:1 Fe<sup>3+</sup>-DFOB-SRFA) were analysed by FTIR. Iron(III) chloride hexahydrate  
198 (FeCl<sub>3</sub>.6H<sub>2</sub>O) was used to prepare the Fe<sup>3+</sup>-complexes. Solid samples for FTIR analysis were  
199 obtained from the acidified aqueous complexes by concentrating the solutes through freeze  
200 drying (Triad LABCONCO with a JAVAC JL-10 high vacuum pump) to minimise infrared  
201 absorption by water and improve peak/band resolution. All samples, including the air-dried  
202 residues from filtration, were prepared for FTIR analysis using the KBr pellet technique  
203 (Prasad et al., 2006), mixing ~1 mg of sample with 100–200 mg spectroscopy grade KBr  
204 (Merck, IR spectroscopy, Uvasol<sup>®</sup>). When not in use, the pellets were stored in a desiccator  
205 to minimise uptake of water. All FTIR data were collected over 200–4000 cm<sup>-1</sup> on a Perkin  
206 Elmer Spectrum One FTIR spectrometer with dedicated spectrum handling software (version  
207 5.0.1). The spectra have a resolution of 4 cm<sup>-1</sup> and are the aggregate of 128 scans.

208

## 209 2.5. SRFA and DFOB quantification

210

211 Filtrate SRFA was quantified by first obtaining a UV-Vis scan (220-900 nm) of a  
212 standard aqueous SRFA solution (31.2 mg SRFA L<sup>-1</sup>) to obtain the  $\lambda_{\max}$  (254 nm). A series of  
213 aqueous SRFA solutions of varying concentration were then prepared to construct the  
214 calibration curve. Aqueous SRFA from each batch dissolution experiment was then  
215 determined by placing 1 mL filtrate in micro cuvettes of 10 mm path length and measuring  
216 UV absorption at 254 nm (Qu et al., 2003; Tatár et al, 2004). Absorbance readings were  
217 obtained on a Shimadzu UV-1800 spectrophotometer fitted with tungsten iodine (visible) and

218 deuterium (UV) lamps. An aliquot of acidified MOPS/NaNO<sub>3</sub> was used to base correct the  
219 UV-Vis spectrophotometer before analysis of batch solutions.

220 Siderophore concentrations in the filtrates from the adsorption experiments were  
221 determined following the chelometric method (Cocozza et al., 2002; Cheah et al., 2003).  
222 Spectrophotometric measurements of the Fe-DFOB complex were obtained at 467 nm within  
223 1 h after filtration. Filtrates and standards were acidified to pH 1.5 to 1.7 with 8 μL 70%  
224 HClO<sub>4</sub> (BDH ARISTAR). We then added 170 μL of 15 mM Fe(ClO<sub>4</sub>)<sub>3</sub> to each filtrate sample  
225 to give an Fe concentration in excess of that needed to complex all DFOB. Analogous  
226 siderophore-free blank solutions containing only MOPS buffer, background electrolyte and  
227 added Fe were likewise acidified to pH 1.5 to 1.7. Subtraction of absorbance for the blank  
228 solution from that for the sample filtrates yielded the net absorbance, which we attribute to  
229 siderophore not adsorbed. The DFOB surface excess (μmol g<sup>-1</sup>) was determined by dividing  
230 the siderophore concentration loss (i.e. 270 μM minus DFOB concentration in the filtrate) by  
231 the goethite concentration. DFOB quantification in system 9 (i.e. DFOB without goethite)  
232 served as a validation step to account for any DFOB sorbed to container walls and filters.

233 UV-Vis spectra were obtained for DFOB, Fe(ClO<sub>4</sub>)<sub>3</sub>, SRFA, Fe<sup>3+</sup>-DFOB, Fe<sup>3+</sup>-SRFA,  
234 DFOB-SRFA and Fe-DFOB-SRFA standard solutions prepared in a MOPS/NaNO<sub>3</sub> matrix  
235 and compared to the spectra of the batch filtrate solutions. Furthermore, the spectrum of a  
236 MOPS/NaNO<sub>3</sub> solution was compared to that of deionized water to ensure that  
237 MOPS/NaNO<sub>3</sub> peaks did not overlap those from Fe-DFOB.

238

## 239 2.6. SEM and AFM imaging

240

241 Goethite morphology was determined before and after reaction with SRFA and  
242 DFOB. Powdered goethite samples were fixed to Al stubs then coated with Au-Pd prior to

243 analysis on a Zeiss Gemini Ultra Plus SEM operating at 5.0 kV and a spot size of 20.00  $\mu\text{m}$   
244 over a range of magnifications to observe gross particle morphology. AFM was used to  
245 determine the surface relief of the goethite crystals. The analysis was conducted using an  
246 Asylum MFP-3D-SA (Santa Barbara, USA) instrument in AC mode. The prepared film  
247 samples ( $1\text{ cm}^2$ ) were placed on glass slides and scanned in air over a  $10 \times 10\ \mu\text{m}^2$  area using  
248 an Olympus AC240TS tip (spring constant  $2\text{ N m}^{-1}$ ). Surface roughness, amplitude and height  
249 channels were monitored and analysed using IGOR PRO software.

250

### 251 3. RESULTS

252

#### 253 3.1. Characterisation of goethite

254

255 The addition of 5 M KOH to 1 M  $\text{Fe}(\text{NO}_3)_3 \cdot 9\text{H}_2\text{O}$  produced a brownish-yellow  
256 precipitate of Munsell colour 10YR 6/8. The precipitates were confirmed as goethite ( $\alpha$ -  
257  $\text{FeOOH}$ ) by comparing their powder X-ray diffraction patterns with those reported in the  
258 International Centre for Diffraction Data® Files (ICDD Files 1081-464). All the peaks  
259 produced by the precipitates related to the structure of goethite; the absence of extraneous  
260 peaks indicated that no other phases were present at detectable levels.

261 Analysis of goethite morphology by SEM showed the crystals to be lath shaped as  
262 observed previously (Cornell et al., 1974; Kosmulski et al., 2004). The fractured appearance  
263 of some crystals we attribute to desiccation and water loss under high vacuum. The height of  
264 the crystals obtained through AFM analysis was  $\sim 60\text{ nm}$ , while the  $\text{N}_2$ -BET surface area was  
265  $43\text{ m}^2\text{ g}^{-1}$ , slightly greater than that reported elsewhere (e.g.  $35 \pm 3\text{ m}^2\text{ g}^{-1}$ ; Kraemer et al.,  
266 1999;  $38\text{ m}^2\text{ g}^{-1}$ ; Carrasco et al., 2007). Sorbed SRFA imparts surface roughness to goethite  
267 and disrupts its characteristic lath-shaped morphology.

268

## 269 3.2. Goethite dissolution

270

271 Iron release kinetics for goethite dissolution in the presence of DFOB and / or SRFA  
272 at 270  $\mu\text{M}$  initial siderophore concentration are shown in Fig. 4. Soluble Fe is detected only  
273 for those systems containing both goethite and DFOB (i.e. systems 1 – 6). At reaction times >  
274 50 h Fe release broadly followed zero-order kinetics, with Fe concentration depending  
275 linearly on time (Table 1). This linearity is commonly observed for far from equilibrium  
276 dissolution reactions (Sposito, 1994; Lasaga, 1998), where the slope of the regression line  
277 equation (Table 1, column 2) is equal to the zero-order rate coefficient. Generally, goethite  
278 suspensions containing both DFOB and SRFA (e.g. systems 4, 5, 6) show increased slopes of  
279 the linear fits and greater soluble Fe than those containing only DFOB (i.e. system 1). This  
280 observation corroborates the complementary work of Reichard et al. (2007a) on two-ligand  
281 systems, who reported increased goethite dissolution at pH 6 in the presence of 50  $\mu\text{M}$  DFOB  
282 alongside 50  $\mu\text{M}$  oxalate, malonate, succinate or fumarate. These workers observed that in  
283 the presence of 50  $\mu\text{M}$  DFOB alone, goethite dissolution yielded  $\sim 5 \mu\text{M}$  Fe, but this  
284 increased to nearly 10  $\mu\text{M}$  Fe with the addition of the above low molecular weight organic  
285 ligands. Furthermore, in our study, addition of SRFA prior to DFOB (i.e. systems 4 and 5)  
286 yielded greater slopes than for those systems where DFOB was introduced prior to SRFA (i.e.  
287 systems 2 and 3). Introduction of the DFOB-SRFA complex to the goethite suspension  
288 (system 6) gave rise to the greatest Fe release.

289 In dissolution reactions under far from equilibrium conditions, the zero-order rate  
290 coefficient is generally considered to be proportional to either: (i) the specific surface area or  
291 (ii) the mass of the dissolving solid (Lasaga, 1998). However, as the normalisation of  
292 dissolution rates with respect to surface area is not straightforward (Brantley and Chen,

293 1995), we express the dissolution rates with respect to mass of the goethite. Mass normalised  
294 rate coefficients ( $\mu\text{mol g}^{-1} \text{h}^{-1}$ ) were therefore derived as the slope of the linear fit divided by  
295 the goethite mass, and these coefficients are presented in column 3 of Table 1. The mass-  
296 normalised dissolution rate coefficients are greatest for those systems containing SRFA,  
297 particularly where this humic material was introduced prior to DFOB. Interestingly, the  
298 simultaneous introduction of DFOB and SRFA as the DFOB-SRFA complex (system 6)  
299 yielded the greatest rate coefficient of all systems.

300 The mass-normalised dissolution rate reported by Coccozza et al. (2002) for the  
301 dissolution of goethite by DFOB at 25 °C (i.e.  $0.135 \mu\text{mol g}^{-1} \text{h}^{-1}$ ) is approximately one-half  
302 that reported here (i.e.  $0.257 \mu\text{mol g}^{-1} \text{h}^{-1}$ ). Some of this difference may arise from the slightly  
303 higher concentration of DFOB used in this study (i.e.  $270 \mu\text{M}$  vs.  $240 \mu\text{M}$ ). However, most of  
304 this difference in dissolution rate can be attributed to variation in the nature of the goethite  
305 sample. Cornell and Schwertmann (2003), for example, cite the influence of goethite  
306 morphology and crystallinity as important determinants of dissolution rate. The goethite used  
307 in this study was prepared using a method broadly similar to that adopted by Coccozza et al.  
308 (2002), with the exception that these earlier workers incorporated a longer aging period  
309 yielding a goethite which, presumably, displayed greater long-range order than that used in  
310 the present study.

311 UV-Vis spectra for untreated batch filtrates are shown in Fig. 5. These spectra reveal  
312 two main regions of absorption: a broad, low peak at 400 – 500 nm which is assigned to  $\text{Fe}^{3+}$ -  
313 DFOB, and another peak at 236 nm which is due to the uncomplexed anionic DFOB species,  
314  $\text{HDFOB}^{2-}$ , whose three hydroxamate groups are deprotonated whilst the terminal amine  
315 remains protonated (Edwards et al., 2005). We disregard other causes for the peak at 236 nm  
316 as UV-Vis scans of reference solutions of SRFA,  $\text{Fe}(\text{ClO}_4)_3$ , MOPS/ $\text{NaNO}_3$ , Fe-DFOB, and  
317 Fe-SRFA did not show any absorption in this region. Thus, the spectra in Fig. 5 indicate that

318 the untreated filtrates contain both complexed DFOB as  $\text{Fe}^{3+}$ -DFOB and uncomplexed  
319 DFOB.

320 The values of surface excess of DFOB on goethite at 25 °C, pH 6.5 and 270  $\mu\text{M}$   
321 initial siderophore concentration are given in Table 1 (column 4) for the six systems  
322 containing both goethite and DFOB. Although we measure surface excess at a single  
323 temperature (i.e. 25 °C) Coccozza et al. (2002) report no significant change in surface excess  
324 of DFOB on goethite over the temperature range 25 °C to 55 °C for a comparable system.  
325 However, the surface excess we calculate for our system 1 (i.e. 14.4  $\mu\text{mol g}^{-1}$ ) is nearly five  
326 times that observed by Coccozza et al. (2002) (i.e. 2.99  $\mu\text{mol g}^{-1}$ ) under comparable  
327 conditions. We again attribute this difference to variation in goethite synthesis procedure,  
328 with attendant variation in crystallite morphology and density of reactive surface OH groups  
329 (Cornell and Schwertmann, 2003).

330 A pseudo-first-order rate coefficient may be used to characterise the kinetics of  
331 ligand-promoted dissolution under far from equilibrium conditions as described by Stumm et  
332 al. (1987). This approach was applied by Coccozza et al. (2002) to demonstrate the  
333 temperature dependence of DFOB mediated goethite dissolution at 55 °C, and the lack of  
334 temperature dependence over the range 25 to 40 °C. For the present study, the coefficient ( $\text{h}^{-1}$ )  
335 was derived as the ratio of the mass-normalised dissolution rate coefficient to the DFOB  
336 surface excess. These values are presented in Table 1 (column 5) and are generally in line  
337 with that reported by Kraemer et al. (1999) (i.e. 0.01  $\text{h}^{-1}$ ). This broad congruence of pseudo-  
338 first-order rate coefficients implies that differences in dissolution rate depend principally on  
339 DFOB surface excess as influenced by reagent addition sequence.

340

### 341 3.3. FTIR spectra

342

343 The dominant FTIR vibrations and corresponding assignments for the Fe-free and  
344 Fe<sup>3+</sup>-complexed standards are shown in Table 2. All FTIR absorption peaks produced by our  
345 synthetic goethite relate to the structure of goethite. The absence of extraneous peaks  
346 indicated that no other phases were present at detectable levels. The FTIR spectrum for our  
347 synthetic goethite (Fig. 6) has an absorption band at 640 cm<sup>-1</sup>, representing the FeO<sub>6</sub> lattice  
348 vibrations (Prasad et al., 2006). Other prominent vibrations are the in-plane ( $\delta$ ) and out-of-  
349 plane ( $\gamma$ ) deformational (bending) modes of hydroxyls at 891 cm<sup>-1</sup> and 795 cm<sup>-1</sup>, respectively  
350 (cf., Prasad et al. 2006). The broad absorption band located at 3132 cm<sup>-1</sup> is assigned to the  
351 hydroxyl stretch of surface OH, previously reported at 3100 – 3150 cm<sup>-1</sup> (Cornell and  
352 Schwertmann, 2003).

353 In the FTIR spectrum for DFOB the terminal N-H stretching vibrations occur at 3128  
354 cm<sup>-1</sup> and 3325 cm<sup>-1</sup>, while the vibrational stretching of the amide I band of the C=O group  
355 occurs at 1624 cm<sup>-1</sup> (Cozar et al., 2006; Siebner-Freibach et al., 2006). Another C=O  
356 absorption band at 1599 cm<sup>-1</sup> represents the hydroxamate C=O (cf., Edwards et al., 2005;  
357 Domagal-Goldman et al., 2009). An absorption band at 1537 cm<sup>-1</sup> arises from the  
358 superposition of N-H bending and C-N stretching vibrations in the amide II group (cf.,  
359 Nightingale and Wagner, 1954) as well as O-H (hydroxamate) in-plane bending vibrations  
360 (Cozar et al., 2006). The band at 1480 cm<sup>-1</sup> is assigned to both the hydroxamate NOH bend  
361 and the C-N oxime (hydroxamate resonance structure) stretch corresponding to the 1470 cm<sup>-1</sup>  
362 band of Edwards et al. (2005) (Fig. 6). We also observed a band at 1386 cm<sup>-1</sup> arising from a  
363 combination of vibrational deformation modes in the hydroxamate group and terminal N (cf.,  
364 1379 cm<sup>-1</sup> Edwards et al., 2005). An additional band, at 1047 cm<sup>-1</sup>, coincides with the  
365 hydroxamate N-O resonance of DFOB. However, this band is not due exclusively to DFOB  
366 as methanesulfonate, the counter-ion of the DFOB mesylate salt, also shows strong  
367 absorption at 1049 cm<sup>-1</sup> (Borer et al., 2009; Simanova et al., 2010).

368 The FTIR spectrum for SRFA (Fig. 6) displayed two prominent absorption bands, at  
369 3425 cm<sup>-1</sup> and 1720 cm<sup>-1</sup>, and these were assigned to the phenolic O-H and protonated  
370 carboxylic acid C=O vibrational stretching modes, respectively (cf., International Humic  
371 Substance Society, 2008). Other absorption bands at 1629 cm<sup>-1</sup> and 1384 cm<sup>-1</sup> represent,  
372 respectively, the deprotonated asymmetric and symmetric vibrational stretching of  
373 carboxylate C=O (cf., Fu and Quan, 2006; Hay and Myneni, 2007). The broad band at 1218  
374 cm<sup>-1</sup>, assigned to the O-H phenolic stretch, was previously observed at 1217 cm<sup>-1</sup> by Fu and  
375 Quan (2006).

376 Complexation between DFOB and Fe<sup>3+</sup> yields a shift in the amide I band to 1622 cm<sup>-1</sup>  
377 from 1624 cm<sup>-1</sup> (Fig. 6) as reported by Edwards et al. (2005). The hydroxamate absorption  
378 bands at 1537 cm<sup>-1</sup> and 1480 cm<sup>-1</sup>, as well as the absorption band at 1386 cm<sup>-1</sup>, assigned to  
379 the hydroxamate near the terminal N, also disappeared upon complexation of DFOB to Fe<sup>3+</sup>.  
380 The Fe<sup>3+</sup>-DFOB complex gave rise to a new vibrational stretching mode at 1568 cm<sup>-1</sup>,  
381 assigned to hydroxamate C=N, and a shift of the existing 1047 cm<sup>-1</sup> band to 1045 cm<sup>-1</sup>,  
382 assigned to hydroxamate N-O (Fig. 6) (Cozar et al., 2006). Upon coordination of  
383 hydroxamate oxygen to Fe<sup>3+</sup>, a new hydroxamate absorption band emerged at 1459 cm<sup>-1</sup>,  
384 previously reported at 1455 cm<sup>-1</sup> by Borer et al. (2009), in a region where bands at 1537 cm<sup>-1</sup>  
385 and 1480 cm<sup>-1</sup> once appeared (Table 2). The Fe<sup>3+</sup>-DFOB complex also gives rise to a band at  
386 561 cm<sup>-1</sup>, reported previously at 555 cm<sup>-1</sup> (Cozar et al., 2006), attributed to the Fe-O  
387 stretching vibration, but distinct from the Fe-O stretching of the goethite lattice. Additionally,  
388 a broad and intense peak at 3368 cm<sup>-1</sup>, accompanied by two small shoulders, we attribute to  
389 the dissociation of the hydroxamate hydroxyl groups following Fe<sup>3+</sup> coordination.

390 Following complexation of Fe<sup>3+</sup> with SRFA, the O-H band at 3425 cm<sup>-1</sup> becomes  
391 broader, and shifts to 3410 cm<sup>-1</sup> (Fig. 6). In contrast, the COOH and asymmetric C=O bands  
392 at 1720 cm<sup>-1</sup> and 1629 cm<sup>-1</sup>, respectively, disappeared, whilst new, slightly lower intensity



393 bands appeared at  $1687\text{ cm}^{-1}$  and  $1631\text{ cm}^{-1}$ . Meanwhile, the peak at  $1384\text{ cm}^{-1}$  became  
394 sharper and more intense following  $\text{Fe}^{3+}$  complexation with SRFA (cf., Fu and Quan, 2006),  
395 indicating the complexation of carboxylate oxygen to  $\text{Fe}^{3+}$ .

396 Our FTIR assignments for the DFOB-SRFA and  $\text{Fe}^{3+}$ -DFOB-SRFA complexes are  
397 based on comparison of the FTIR spectra for DFOB, SRFA,  $\text{Fe}^{3+}$ -DFOB,  $\text{Fe}^{3+}$ -SRFA, DFOB-  
398 SRFA and  $\text{Fe}^{3+}$ -DFOB-SRFA. Upon formation of the DFOB-SRFA complex, the SRFA  
399 phenolic absorption band at  $3425\text{ cm}^{-1}$  becomes less intense and slightly broader, shifting to  
400  $3417\text{ cm}^{-1}$ , while another phenolic band at  $1216\text{ cm}^{-1}$  shifted to  $1218\text{ cm}^{-1}$  (Fig. 6). The  
401 intensity of the prominent SRFA carboxylic C=O band at  $1720\text{ cm}^{-1}$  decreased significantly  
402 and shifted to  $1719\text{ cm}^{-1}$ , whilst the asymmetric C=O band at  $1629\text{ cm}^{-1}$  shifted to  $1626\text{ cm}^{-1}$ .  
403 With respect to the DFOB, bands assigned to the terminal amines shifted from  $3128\text{ cm}^{-1}$  and  
404  $3325\text{ cm}^{-1}$  to a single band at  $2939\text{ cm}^{-1}$  of lower intensity.

405 Formation of the  $\text{Fe}^{3+}$ -DFOB-SRFA complex changed the FTIR spectra for both  
406 SRFA and DFOB (Fig. 6). The intensity of the SRFA carboxylic C=O band was reduced,  
407 shifting from  $1720$  to  $1723\text{ cm}^{-1}$ , while the SRFA symmetric C=O absorption band at  $1384$   
408  $\text{cm}^{-1}$  disappeared. The SRFA phenolic OH band at  $1216\text{ cm}^{-1}$  remained largely as it was in  
409 the DFOB-SRFA complex, whilst the asymmetric stretching of the carboxylate C=O  
410 increased from  $1629\text{ cm}^{-1}$  in the Fe-free complex to  $1642\text{ cm}^{-1}$  in the  $\text{Fe}^{3+}$ -DFOB-SRFA  
411 complex. The phenolic OH band shifted from  $3425\text{ cm}^{-1}$  for the Fe-free SRFA to  $3437\text{ cm}^{-1}$   
412 for the  $\text{Fe}^{3+}$ -DFOB-SRFA complex. The N-O resonance of the hydroxamate group decreased  
413 from  $1047\text{ cm}^{-1}$  in DFOB to  $1042\text{ cm}^{-1}$  in the  $\text{Fe}^{3+}$ -DFOB-SRFA complex and was  
414 accompanied by considerable peak sharpening. Furthermore, the Fe-O vibration at  $561\text{ cm}^{-1}$   
415 indicating complexation between  $\text{Fe}^{3+}$  and DFOB was observed at  $542\text{ cm}^{-1}$  in the ternary  
416 complex (Fig. 6). Weak bands at  $3010\text{ cm}^{-1}$  and  $2954\text{ cm}^{-1}$  for the  $\text{Fe}^{3+}$ -DFOB-SRFA  
417 complex are likely due to the decrease in frequency of the N-H group of the terminal N in the

418 DFOB as a result of electrostatic interaction between the DFOB terminal amine and charged  
419 SRFA groups.

420

## 421 4. DISCUSSION

422

### 423 4.1. Sorption of SRFA and DFOB to goethite

424

425 Adsorption of organic matter to iron oxide surfaces occurs by electrostatic  
426 interactions, ligand exchange, hydrogen bonding and van der Waals interactions (Sposito,  
427 1984). Coulombic attraction of organic solutes to metal oxides can be predicted through  
428 construction of a Schindler diagram, a banded rectangle in which the charge properties of the  
429 adsorptive and adsorbent are compared as a function of solution pH (Fig. 7) (Schindler,  
430 1990). The bottom rectangle displays a horizontal line indicating the pH range over which  
431 adsorption is expected to occur based solely on charge. Adsorption occurring outside of this  
432 range implies the involvement of specific adsorption mechanisms. On the basis of the  
433 Schindler diagram depicted in Fig. 7a, adsorption of SRFA to goethite is predicted over pH ~  
434 3 to 9.

435 At pH 6.5 and an initial SRFA concentration of  $11.6 \text{ mg C L}^{-1}$ , the surface excess of  
436 SRFA on goethite was  $0.33 \text{ mg m}^{-2}$ . This value compares favourably with that reported by  
437 Filius et al. (2000) for fulvate adsorption to goethite at pH 7 (i.e.  $0.3 \text{ mg FA g}^{-1}$ ) and also  
438 Weng et al. (2006) for their system at pH 5.5 (i.e.  $0.4 \text{ mg FA g}^{-1}$ ). FTIR spectra for the  
439 goethite-SRFA surface association were too complex to derive useful molecular-level  
440 information concerning adsorption mechanisms. However, FTIR spectra for aqueous  $\text{Fe}^{3+}$ -  
441 SRFA species, when compared with spectra for several reference aqueous complexes (Fig.  
442 6), revealed that  $\text{Fe}^{3+}$  forms inner-sphere complexes with COOH and phenolic OH of SRFA,

443 consistent with that reported in previous studies (Fu and Quan, 2006; Hay and Myeni, 2007).  
444 Furthermore, application of the charge distribution multi-site complexation (CD-MUSIC)  
445 model provides theoretical evidence that carboxylic groups of SRFA form inner-sphere  
446 complexes with Fe via the singly coordinated surface hydroxyls of goethite (i.e. those  
447 hydroxyls coordinated to a single  $\text{Fe}^{3+}$  cation) (Weng et al., 2005; Weng et al., 2006). On the  
448 basis of these theoretical predictions and our experimental data, we propose that SRFA binds  
449 to the goethite surface via inner-sphere complexation as depicted in Fig. 8, corroborating the  
450 work of Filius et al. (2000), who observed inner-sphere adsorption of fulvic acid at pH below  
451 the PZC for goethite. Importantly, SRFA adsorption lowers the PZC of goethite and reduces  
452 positive surface charge in the vicinity of the adsorption site (Tipping and Cooke, 1982).

453         The Schindler diagram shown in Fig. 7b predicts that goethite can serve as an  
454 effective sorbent for DFOB only at pH  $\sim$  8 to 9. However, for our systems at pH 6.5, we  
455 observe a surface excess of DFOB ranging from 14.4 to 26.5  $\mu\text{mol g}^{-1}$  (Table 1). Much of this  
456 DFOB will be adsorbed via inner-sphere surface complexes (Carrasco et al., 2007), however  
457 electrostatic factors may be significant in increasing overall uptake. The predicted  
458 electrostatic repulsion at pH 6.5 between DFOB ( $\text{pK}_a \sim 8.6$ ) and the positively charged  
459 goethite surface (PZC = 9.2) can be minimised through orientation of the approaching  
460 siderophore such that the hydroxamate group furthest from the protonated amine makes first  
461 contact with the surface (Cocozza et al., 2002). More significantly, adsorption of the anionic  
462 SRFA reduces the positive surface charge of goethite near the site of adsorption (Tipping and  
463 Cooke, 1982), thus facilitating localised uptake of DFOB. Consistent with the predicted  
464 SRFA enhanced uptake of DFOB, our data show that those systems with both SRFA and  
465 DFOB give rise to greater DFOB surface excess than system 1, which contains only DFOB  
466 (Table 1).

467

## 468 4.2. Aqueous complexes

469

470 UV-Vis spectroscopic analysis confirmed the presence of the  $\text{Fe}^{3+}$ -DFOB complex in  
471 supernatant solutions from batch dissolution experiments (Fig. 5). The emergence of FTIR  
472 absorption bands at  $1459\text{ cm}^{-1}$  and  $561\text{ cm}^{-1}$ , assigned to Fe-O (Table 2; Fig. 6), following  
473 formation of the  $\text{Fe}^{3+}$ -DFOB complex provides evidence for presence of the Fe-hydroxamate  
474 bond as depicted in Fig. 1b. These observations are consistent with predictions based on the  
475 high affinity of desferrioxamine B for the  $\text{Fe}^{3+}$  cation ( $K = 10^{31}$ ) (Kraemer, 2004).

476 The absence of both soluble Fe and the  $\text{Fe}^{3+}$ -SRFA species in the supernatant  
477 solutions of system 7 indicates that goethite dissolution does not occur at detectable levels in  
478 the presence of SRFA alone at pH 6.5 (Fig. 4). However, FTIR analysis of model compounds  
479 reveals the diagnostic absorption bands that indicate presence of the  $\text{Fe}^{3+}$ -SRFA complex, a  
480 species that may well form following the liberation of  $\text{Fe}^{3+}$  by DFOB. The most significant  
481 FTIR band arising from the complexation of SRFA with Fe is due to changes in the  
482 carboxylate C=O vibration, appearing at  $1687\text{ cm}^{-1}$  in  $\text{Fe}^{3+}$ -SRFA and  $1720\text{ cm}^{-1}$  in Fe-free  
483 SRFA. Fu and Quan (2006) observed similar changes in C=O vibrations when FA was sorbed  
484 to haematite. The other functional group indicative of  $\text{Fe}^{3+}$ -SRFA bonding, the phenolic OH,  
485 changes from  $3425\text{ cm}^{-1}$  in the uncomplexed SRFA to  $3410\text{ cm}^{-1}$  for  $\text{Fe}^{3+}$ -SRFA (Table 2).

486 Localisation of Fe within the ternary Fe-DFOB-SRFA complex can help to reveal the  
487 mechanisms of goethite dissolution when both organic ligands are present. The FTIR  
488 absorption band most diagnostic of Fe complexation by SRFA arises from the carboxylate  
489 C=O vibration which, when complexed to Fe, decreases from  $1720\text{ cm}^{-1}$  to  $1687\text{ cm}^{-1}$ . In the  
490 ternary complex this vibration occurs at  $1723\text{ cm}^{-1}$  (Table 2), broadly similar to that of the  
491 Fe-free SRFA. Furthermore, we observe the main band representing the  $\text{Fe}^{3+}$ -DFOB  
492 complex, the Fe-O vibration, is also present for the Fe-DFOB-SRFA complex, although

493 occurring at the somewhat lower frequency of  $542\text{ cm}^{-1}$ . On the basis of these spectroscopic  
494 observations we infer that Fe in the ternary complex is bound only to the hydroxamate groups  
495 of DFOB. Thus, in the presence of both DFOB and SRFA, dissolved  $\text{Fe}^{3+}$  is complexed by  
496 DFOB rather than SRFA, consistent with our observations, and as predicted by the much  
497 higher affinity of  $\text{Fe}^{3+}$  for DFOB than for SRFA at pH 6.5 (Pandeya, 1993; Kraemer, 2004;  
498 Muller and Batchelli, 2011). The FTIR spectrum for Fe-DFOB-SRFA also shows notable  
499 increases in wavenumber for SRFA phenolic OH ( $3437\text{ cm}^{-1}$ ) and C=O ( $1642\text{ cm}^{-1}$ ),  
500 compared to their uncomplexed form (Table 2). However, we believe these wavenumber  
501 shifts are not due to Fe complexation by SRFA but rather to ring strain caused by a change in  
502 SRFA conformation to accommodate the DFOB molecule as the Fe-O complex forms  
503 (Sharma, 2007).

504 FTIR data show that SRFA and DFOB combine to form intimate associations in  
505 aqueous solution. Specifically, bonding between the SRFA phenolic OH and the residual  
506 positive charge on the DFOB terminal  $\text{NH}_3$  group yields a significant wavenumber change  
507 for these groups, shifting the uncomplexed SRFA phenolic OH from  $3425\text{ cm}^{-1}$  to  $3417\text{ cm}^{-1}$   
508 in the DFOB-SRFA complex (Table 2). Curiously, the SRFA phenolic OH appears to  
509 dominate these associations, despite the greater population of carboxyl groups within this  
510 humic material, with reports of carboxyl:phenol molar ratios varying from 3:2 (Alvarez-  
511 Puebla et al., 2006) to 4:1 (Ritchie and Perdue, 2003). The FTIR bands for the DFOB  
512 terminal  $\text{NH}_3$  group vibrations display even greater wavenumber shifts, from  $3128\text{ cm}^{-1}$  and  
513  $3325\text{ cm}^{-1}$  in the uncomplexed siderophore to a single absorption peak at  $2939\text{ cm}^{-1}$  in the  
514 DFOB-SRFA complex.

515

516 4.3. Influence of DFOB and SRFA on goethite dissolution

517

518 DFOB adsorbs to goethite principally via inner-sphere surface complexes (Carrasco et  
519 al., 2007), the necessary first step in ligand-controlled dissolution. The rate law for ligand-  
520 controlled dissolution predicts that the mass-normalised dissolution rate of goethite,  $R_{\text{DFOB}}$ ,  
521 will be proportional to the DFOB surface excess,  $n_{\text{DFOB}}$ :

522

$$523 \quad R_{\text{DFOB}} = k_{\text{DFOB}} n_{\text{DFOB}}$$

524

525 where  $k_{\text{DFOB}}$  is a pseudo first-order rate coefficient. The dissolution of goethite by  
526 siderophores obeys this rate law under many experimental conditions, even in the presence of  
527 low MW organic ligands such as oxalate (Cheah et al., 2003). Our values for  $k_{\text{DFOB}}$  show  
528 little variation irrespective of treatment ( $0.012 - 0.020 \text{ h}^{-1}$ ) (Table 1, column 5) and are  
529 broadly in line with that reported by Kraemer et al. (1999) (i.e.  $0.01 \text{ h}^{-1}$ ). However, the  
530 pseudo first-order rate coefficient for dissolution of goethite by DFO-D1, the acetyl  
531 derivative of DFOB, increases to  $0.05 \text{ h}^{-1}$  (Kraemer et al., 1999) while that for a simple  
532 monohydroxamate ligand, acetohydroxamic acid, was calculated as  $0.073 \text{ h}^{-1}$  (Holmén and  
533 Casey, 1998).

534 In the present study, Fe release from goethite increased with the addition of SRFA,  
535 particularly where SRFA is added prior to DFOB (systems 4 and 5), and further still when  
536 SRFA is introduced as the DFOB-SRFA complex (system 6) (Fig. 4). A quantitative  
537 assessment of the effect of SRFA presence on goethite dissolution can be obtained through  
538 comparison of the mass-normalised zero-order rate coefficients (Table 1, column 3). The rate  
539 coefficients for systems 4 ( $0.364 \mu\text{mol g}^{-1} \text{ h}^{-1}$ ) and 5 ( $0.412 \mu\text{mol g}^{-1} \text{ h}^{-1}$ ) are 40 to 60% larger  
540 than that for system 1 ( $0.257 \mu\text{mol g}^{-1} \text{ h}^{-1}$ ), while the coefficient for system 6 ( $0.440 \mu\text{mol g}^{-1}$   
541  $\text{h}^{-1}$ ) is nearly 70% larger than for the SRFA-free system.

542 Despite the positive influence of SRFA on goethite dissolution by means of increased  
543 adsorption of DFOB (compare DFOB surface excess for system 1 with that for systems 2 – 6;  
544 Table 1, column 4), the rate of Fe release does not correlate linearly with DFOB surface  
545 excess. This nonlinear relationship between DFOB adsorption and goethite dissolution may  
546 reflect changes in surface speciation of DFOB when SRFA is present. The SRFA induced  
547 reduction in positive surface charge enables greater electrostatic adsorption of DFOB as  
548 predicted by Tipping and Cooke (1982). However, as formation of a DFOB inner-sphere  
549 complex is the required first step in ligand-controlled dissolution of goethite, DFOB held  
550 non-specifically through Coulombic forces would not contribute to goethite dissolution.  
551 Furthermore, in the case of system 6, inner-sphere complexation of DFOB to goethite may be  
552 partly limited by the rate at which DFOB and SRFA decouple. Nevertheless, the effect of  
553 SRFA presence on the DFOB-goethite system has important implications for the microbial  
554 acquisition of Fe in soils and other humic rich environments. Data in Fig. 4 show that for  
555 nearly all systems the efficacy of DFOB is increased with SRFA presence. For example, at  
556 reaction times of 120 and 330 h, system 1 (with only DFOB) yields 34.7 and 70.3  $\mu\text{M}$  Fe  
557 while system 6 (containing both DFOB and SRFA) yields 71.6 and 125.7  $\mu\text{M}$  Fe,  
558 respectively (Fig. 4). Thus, the benefit to the microbe producing the siderophore is  
559 substantial, and this advantage is achieved with little or no energetic cost to the organism.

560

#### 561 4.4. Mechanism of SRFA enhanced goethite dissolution

562

563 Various mechanisms have been proposed to explain the effect of low MW organic  
564 acids on goethite dissolution by DFOB. For example, in their examination of the oxalate-  
565 DFOB-goethite system at pH 5, Cheah et al. (2003) suggest that Fe solubilised from the  
566 goethite surface by oxalate is subsequently wrested from the  $\text{Fe}^{3+}$ -oxalate aqueous complex

567 by DFOB. Given sufficient DFOB to complex soluble Fe, oxalate will thus be liberated to  
568 react once again with the goethite surface. Reichard et al. (2007a), also examining the  
569 oxalate-DFOB-goethite system, proposed a dissolution mechanism broadly similar to that of  
570 Cheah et al. (2003), except that the former workers identified two distinct pools of labile Fe,  
571 namely, (i)  $\text{Fe}^{3+}$  present as a residuum of goethite synthesis and (ii) kinetically labile  $\text{Fe}^{3+}$   
572 coordinated to unshared hydroxyls. The mechanism we propose here for the dissolution of  
573 goethite in the presence of DFOB and the higher MW organic compound, SRFA, differs from  
574 those proposed for oxalate in that SRFA plays a largely indirect, though no less important  
575 role in increasing the efficacy of DFOB. Adsorbed SRFA reduces the net positive surface  
576 charge of goethite, thereby increasing DFOB uptake, and also, through formation of Fe  
577 complexes with fulvic carboxyl and phenol groups, increases the pool of labile surface Fe.  
578 Our model for goethite dissolution by DFOB in the presence of SRFA, illustrated in Fig. 9, is  
579 summarised below:

580

581 (i) surface Fe of goethite is coordinated to SRFA via carboxylic  $(\text{GOE})\text{Fe}^{3+}-\text{OOC}(\text{SRFA})$  or  
582 phenolic  $(\text{GOE})\text{Fe}^{3+}-\text{O}(\text{SRFA})$  functional groups through ligand exchange;

583

584 (ii) the  $\text{Fe}^{3+}$ -SRFA attachment destabilises Fe-O bonds at the goethite surface, leading to  
585 labilisation of  $\text{Fe}^{3+}$ ;

586

587 (iii) adsorbed SRFA locally reduces the positive charge on the goethite surface, thereby  
588 enhancing  $\text{DFOB}^+$  uptake;

589

590 (iv) protons are displaced from the hydroxamate groups of DFOB as these groups bind to the  
591 labile  $\text{Fe}^{3+}$  via ligand exchange;



592

593 (vi) the  $\text{Fe}^{3+}$ -DFOB<sup>+</sup> complex is released to solution where it remains a free species or  
594 subsequently complexes with aqueous SRFA.

595

596

## 5. CONCLUSIONS

597

598 Our results show that dissolution of goethite by DFOB is enhanced considerably  
599 through the presence of FA, particularly when FA sorption precedes that of DFOB, or when  
600 the two organic compounds are sorbed simultaneously. Importantly, our batch dissolution  
601 experiments incorporating FA reveal a more complex picture of siderophore function than is  
602 portrayed in the current literature. This humic material is revealed as a catalyst for goethite  
603 dissolution, in the sense that FA enhances the efficacy of DFOB but is itself not directly  
604 involved in Fe solubilisation. This work shines important new light on the factors influencing  
605 Fe acquisition by microorganisms and plants in soils and sediments, environments in which  
606 humic materials are ubiquitous. The incorporation of natural organic matter such as FA into  
607 geochemical models of siderophore function is therefore essential to more accurately predict  
608 the geochemical cycling of Fe in these natural environments.

609

610

611

## ACKNOWLEDGEMENTS

612

613 Funding for this study was provided through a Birkbeck, University of London, Research  
614 Studentship and from The Natural History Museum. We thank the following for their  
615 generous assistance: Stanislav Strekopytov, Catherine Unsworth and Emma Williams for  
616 chemical analysis, Agnieszka Dybowska and Hazel Hunter for FTIR spectroscopy, Alex Ball

617 for SEM analysis and photography, Superb Misra for AFM analysis and photography, and  
618 Jens Najorka for XRD analysis.

619

620

## REFERENCES

621

622 Alvarez-Puebla R.A., Valenzuela-Calahorro C. and Garrido J.J. (2006) Theoretical study on  
623 fulvic acid structure, conformation and aggregation - A molecular modelling approach.  
624 *Sci. Total Environ.* 358, 243–254.

625 Borer P., Hug S.J., Sulzberger B., Kraemer S.M. and Kretzschmar R. (2009) ATR-FTIR  
626 spectroscopic study of the adsorption of desferrioxamine B and aerobactin to the surface  
627 of lepidocrocite ( $\gamma$ -FeOOH). *Geochim. Cosmochim. Acta* 73, 4661-4672.

628 Brantley S.L. and Chen Y. (1995) Chemical weathering rates of pyroxenes and amphiboles.  
629 *Rev. Mineral.* 31, 119-172.

630 Carrasco N., Kretzschmar R., Pesch M.-L. and Kraemer S.M. (2007) Low concentrations of  
631 surfactants enhance siderophore-promoted dissolution of goethite. *Environ. Sci. Technol.*  
632 41, 3633-3638.

633 Cervini-Silva J. (2008) Adsorption of trihydroxamate and catecholate siderophores on alpha-  
634 iron (hydr)oxides and their dissolution at pH 3.0 to 6.0. *Soil Sci. Soc. Am. J.* 72, 1557-  
635 1562.

636 Cheah S., Kraemer S.M., Cervini-Silva J. and Sposito G. (2003) Steady-state dissolution  
637 kinetics of goethite in the presence of desferrioxamine B and oxalate ligands: implications  
638 for the microbial acquisition of iron. *Chem. Geol.* 198, 63-75.

639 Chin Y., Aiken G. and O'Loughlin E. (1994) Molecular weight, polydispersity, and  
640 spectroscopic properties of aquatic humic substances. *Environ. Sci. Technol.* 28, 1853–  
641 1858.

642 Coccozza C., Tsao C.C.G., Cheah F., Kraemer S.M., Raymond K.N., Miano T.M. and Sposito  
643 G. (2002) Temperature dependence of goethite dissolution promoted by trihydroxamate  
644 siderophores. *Geochim. Cosmochim. Acta* 66, 431-438.

645 Colnaghi Simionato A.V., Cantú M.D. and Carrilho E. (2006) Characterization of metal-  
646 deferroxamine complexes by continuous variation method: A new approach using  
647 capillary zone electrophoresis. *Microchem. J.* 82, 214-219.

648 Cornell R.M., Posner A.M. and Quirk J.P. (1974) Crystal morphology and the dissolution of  
649 goethite. *J. Inorg. Nucl. Chem.* 36, 1937-1946.

650 Cornell R.M. and Schwertmann U. (2003) *The Iron Oxides - Structure, Properties, Reactions,*  
651 *Occurrences and Uses*, Second Edition. Wiley-VCH, New York.

652 Cozar O., Leopold N., Jelic C., Chis V., David L., Mocanu A. and Tomoaia-Cotisel M.  
653 (2006) IR, Raman and surface-enhanced Raman study of desferrioxamine B and its Fe(III)  
654 complex, ferrioxamine B. *J. Mol. Struct.* 788, 1-6.

655 Cramer S.M., Bryon N. and Csaba H. (1984) High-performance liquid chromatography of  
656 deferroxamine and ferrioxamine: interference by iron present in the chromatographic  
657 system. *J. Chromatogr. A* 295, 405-411.

658 Dhungana S., White P.S. and Crumblis A.L. (2001) Crystal structure of ferrioxamine B: a  
659 comparative analysis and implications for molecular recognition. *J. Biol. Inorg. Chem.* 8,  
660 810-818.

661 Domagal-Goldman S.D., Paul K.W., Sparks D.L. and Kubicki J.D. (2009) Quantum chemical  
662 study of the Fe(III)-desferrioxamine B siderophore complex - Electronic structure,  
663 vibrational frequencies, and equilibrium Fe-isotope fractionation. *Geochim. Cosmochim.*  
664 *Acta* 73, 1-12.

665 Dubbin W.E. and Ander E.L. (2003) Influence of microbial hydroxamate siderophores on  
666 Pb(II) desorption from  $\alpha$ -FeOOH. *Applied Geochemistry* 18, 1751-1756.

667 Edwards D.C., Nielsen S.B., Jarzecki A.A., Spiro T.G. and Myneni S.C.B. (2005)  
668 Experimental and theoretical vibrational spectroscopy studies of acetohydroxamic acid  
669 and desferrioxamine B in aqueous solution: Effects of pH and iron complexation.  
670 *Geochim. Cosmochim. Acta* 69, 3237-3248.

671 Filius J.D., Lumsdon D.G., Meeussen J.C.L., Hiemstra T. and van Riemsdijk W.H. (2000)  
672 Adsorption of fulvic acid on goethite. *Geochim. Cosmochim. Acta* 64, 51-60.

673 Filius J.D., Meeussen J.C.L., Lumsdon D.G., Hiemstra T. and van Riemsdijk W.H. (2003)  
674 Modeling the binding of fulvic acid by goethite: the speciation of adsorbed FA molecules.  
675 *Geochim. Cosmochim. Acta* 67, 1463-1474.

676 Fu H. and Quan X. (2006) Complexes of fulvic acid on the surface of hematite, goethite, and  
677 akaganeite: FTIR observation. *Chemosphere* 63, 403-410.

678 Gan D., Kotob S.I. and Walia D.S. (2007) Evaluation of a spectrophotometric method for  
679 practical and cost effective quantification of fulvic acid. *Ann. Environ. Sci.* 1, 11–15.

680 Ghabbour E.A. and Davies G. (2009) Spectrophotometric analysis of fulvic acid solutions - A  
681 second look. *Ann. Environ. Sci.* 3, 131–138.

682 Haselwandter K. (2008) Structure and function of siderophores produced by mycorrhizal  
683 fungi. *Mineral. Mag.* 72, 61-64.

684 Hay M.B. and Myneni S.C.B. (2007) Structural environments of carboxylic groups in natural  
685 organic molecules from terrestrial systems. Part 1: infrared spectroscopy.  
686 *Geochim. Cosmochim. Acta* 71, 3518-3532.

687 Holmén B.A. and Casey W.H. (1996) Hydroxamate ligands, surface chemistry and the  
688 mechanism of ligand promoted dissolution of goethite [ $\alpha$ -FeOOH(s)].  
689 *Geochim. Cosmochim. Acta* 60, 4403-4416.

690 Holmén B.A. and Casey W.H. (1998) Erratum to Hydroxamate ligands, surface chemistry  
691 and the mechanism of ligand promoted dissolution of goethite [ $\alpha$ -FeOOH(s)].  
692 *Geochim. Cosmochim. Acta* 62, 726.

693 International Humic Substance Society (2008) FTIR spectra were measured at the Instituto di  
694 Chimica Agraria, Università di Bari, Bari, Italy. [online] Available at:  
695 <<http://www.humicsubstances.org/spectra.html>> [Accessed on 25<sup>th</sup> June, 2012].

696 Kosmulski M., Durand-Vidal S., Maczaka E. and Rosenholm J. (2004) Morphology of  
697 synthetic goethite particles. *J. Colloid Interf. Sci.* 271, 261-269.

698 Kraemer S.M. (2004) Iron oxide dissolution and solubility in the presence of siderophores.  
699 *Aquat. Sci.* 66, 3-18.

700 Kraemer S.M., Cheah S., Zapf R., Xu J., Raymond K.N. and Sposito G. (1999) Effect of  
701 hydroxamate siderophore on Fe release and Pb(II) adsorption by goethite.  
702 *Geochim. Cosmochim. Acta* 63, 3003-3008.

703 Lasaga A.C. (1998) *Kinetic Theory in the Earth Sciences*. Princeton University Press.

704 Liermann L.J., Kalinowski B.E., Brantley S.L. and Ferry J.G. (2000) Role of bacterial  
705 siderophores in dissolution of hornblende. *Geochim. Cosmochim. Acta* 64, 587-602.

706 Muller F. and Batchelli S. (2011) Binding of iron and copper to humic colloids in the Thurso  
707 River plume. *Geophys. Res. Abstr.* 13, EGU2011-8132.

708 Nightingale R.E., Wagner E.L. (1954) The vibrational spectra and structure of solid  
709 hydroxylamine and deuterio-hydroxylamine. *J. Chem. Phys.* 22, 203–207.

710 Pandeya S.B. (1993) Ligand competition method for determining stability constants of fulvic  
711 acid iron complexes. *Geoderma* 58, 219–231.

712 Powell P.E., Cline G.R., Reid C.P.P. and Szanislo P.J. (1980) Occurrence of hydroxamate  
713 siderophore iron chelators in soils. *Nature* 287, 833–834.

714 Prasad P.S.R., Prasad K.S., Chaitanya V.K., Babu E.V.S.S.K., Sreedhar B. and Murthy S.R.  
715 (2006) In situ FTIR study on the dehydration of natural goethite. *J. Asian Earth Sci.* 27,  
716 503-511.

717 Qu J.-H., Liu H.-J., Liu S.-X. and Lei P.J. (2003) Reduction of fulvic acid in drinking water  
718 by ferrate. *J Environ. Eng.-ASCE* 129, 17-24.

719 Raymond K.N. and Dertz E.A. (2004) Biochemical and physical properties of siderophores.  
720 In *Iron Transport in Bacteria* (eds. A.R. Mew, S.M. Payne and J.H. Crosa). ASM Press,  
721 Washington, pp. 3 - 17.

722 Reichard P.U., Kretzschmar R. and Kraemer S.M. (2007a) Dissolution mechanisms of  
723 goethite in the presence of siderophores and organic acids. *Geochim. Cosmochim. Acta* 71,  
724 5635-5650.

725 Reichard P.U., Kretzschmar R. and Kraemer S.M. (2007b) Rate laws of steady-state and non-  
726 steady-state ligand-controlled dissolution of goethite. *Colloid Surface A* 306, 22-28.

727 Ritchie J.D. and Perdue E.M. (2003) Proton-binding study of standard and reference fulvic  
728 acid, humic acids, and natural organic matter. *Geochim. Cosmochim. Acta* 67, 85-96.

729 Schindler P.W. (1990) Co-adsorption of Metal Ions and Organic Ligands: Formation of  
730 Ternary Complexes. In *Mineralogy Volume 23 Mineral-Water Interface Geochemistry*  
731 (eds. M.F. Hochella and A.F. White). Mineralogical Society of America, Washington, DC.  
732 Chapter 7.

733 Schwertmann U. and Cornell R.M. (1991) *Iron Oxides in the Laboratory: Preparation and*  
734 *Characterisation*. VCH Publishers, New York.

735 Sharma B.K. (2007) *Fundamental Principles of Spectroscopy*. Krishna Prakashan Media Ltd,  
736 Delhi.

737 Siebner-Freibach H., Hadar Y., Yariv S., Lapidés I. and Chen Y. (2006)  
738 Thermospectroscopic study of the adsorption mechanism of the hydroxamic siderophore  
739 ferrioxamine B by calcium montmorillonite. *J Agric Food Chem.* 54, 1399-1408.

740 Simanova A.A., Persson P. and Loring J.S. (2010) Evidence for hydrolysis and Fe(III)  
741 reduction in the dissolution of goethite by desferrioxamine-B. *Geochim.Cosmochim. Acta*  
742 74, 6706-6720.

743 Sposito G. (1984) *The Surface Chemistry of Soils*. Oxford University Press, New York.

744 Sposito G. (1994) *Chemical Equilibria and Kinetics in Soils*. Oxford University Press, New  
745 York. .

746 Stevenson R.J. (1985) Geochemistry of Soil Humic Substances. In *Humic Substances in Soil,*  
747 *Sediment and Water- Geochemistry, Isolation and Characterisation* (eds. G.R. Aiken,  
748 D.M. McKnight and R.L. Wershaw). John Wiley and Sons, New York.

749 Stumm W., Wehrli B. and Wieland E. (1987) Surface complexation and its impact on  
750 geochemical kinetics. *Croat. Chem. Acta* 50, 1861-1869.

751 Tatár E., Mihucz V.G., Zámbo L., Gasparics T. and Zárny G. (2004) Seasonal changes of  
752 fulvic acid, Ca and Mg concentrations of water samples collected above and in the Béke  
753 Cave of the Aggtelek karst system (Hungary). *Appl. Geochem.* 19, 1727-1733.

754 Tipping E. and Cooke D. (1982) The effects of adsorbed humic substances on the surface  
755 charge of goethite ( $\alpha$ -FeOOH) in fresh waters. *Geochim.Cosmochim. Acta* 46, 75-80.

756 Watteau F. and Berthelin J. (1994) Microbial dissolution of iron and aluminium from soil  
757 minerals: efficiency and specificity of hydroxamate siderophores compared to aliphatic  
758 acids. *Eur. J. Soil Biol.* 30, 1–9.

759 Weng L.P., Koopal L.K., Hiemstra T., Meeussen J.C.L. and Van Riemsdijk W.H. (2005)  
760 Interactions of calcium and fulvic acid at the goethite-water interface.  
761 *Geochim.Cosmochim. Acta* 69, 325-339.

762 Weng L.P., Van Riemsdijk W.H., Koopal L.K. and Hiemstra T. (2006) Adsorption of humic  
763 substances on goethite: Comparison between humic acids and fulvic acids. *Environ. Sci.*  
764 *Technol.* 40, 7494-7500.

765 Whitnall M. and Richardson D.R. (2006) Iron: A new target for pharmacological intervention  
766 in neurodegenerative diseases. *Semin. Pediatr. Neurol.* 13, 186–187.

767

768

769

770

771

772

773

774

775

776

777

778

779

780

781

782

783

784

785

786



787 Figure Captions

788

789 Figure 1. (a) Structural representation of desferrioxamine-B (DFOB). The terminating R  
790 group (i) is an amine ( $pK_a = 10.9$ ). The three hydroxyl groups (ii – iv) have  $pK_a$  values of 9.8,  
791 9.2 and 8.6, respectively (Colnaghi Simionato et al., 2006). The hydroxamate (oxime) group  
792 is shown along with the amide I (C=O) and amide II (N-H and C-N). Adapted from Whitnall  
793 and Richardson (2006). (b) Structure of DFOB bound to  $Fe^{3+}$  as ferrioxamine B. DFOB is  
794 hexadentate, giving a complex with  $Fe^{3+}$  comprised of three, five-membered rings. Adapted  
795 from Cramer et al. (1984).

796

797 Figure 2. Generalised depiction of the proposed molecular structure of FA based on the  
798 Temple-Northeastern-Birmingham (TNB) molecular modelling programme (Alvarez-Puebla  
799 et al. (2006), in accordance with the experimentally derived elemental composition, number  
800 and type of acidic groups, and molecular weight of FA.

801

802 Figure 3. Graphical representation showing the permutations of the batch dissolution of  
803 goethite with DFOB and SRFA as a function of reaction duration.

804

805 Figure 4. Iron release by goethite in the presence of only DFOB (system 1) and both DFOB  
806 and SRFA (systems 2 – 6), with permutations as described in Fig. 3. System 7 is a goethite-  
807 SRFA suspension; system 8 is a goethite suspension lacking any organic ligand. Systems 9  
808 and 10 are solutions of DFOB and SRFA, respectively, and serve as controls. Initial  
809 siderophore concentration: 270  $\mu M$ ; solid concentration: 0.7  $g L^{-1}$ ; pH 6.5.

810

811

812

813 Figure 5. UV-Vis spectra of untreated filtrate solutions showing absorbance for uncomplexed  
814 DFOB (270  $\mu$ M) near 236 nm and absorbance for the Fe-DFOB complex appearing as a low,  
815 broad peak at 400 – 500 nm.

816

817 Figure 6. FTIR spectra for synthetic goethite, DFOB, SRFA, Fe-DFOB, Fe-SRFA, DFOB-  
818 SRFA and Fe-DFOB-SRFA. Reference compounds have the following molar ratios:-  
819 Fe:DFOB (2:1), Fe:SRFA (5:1), DFOB:SRFA (1:1) and Fe:DFOB:SRFA (5:1:1). See Table  
820 2 for peak assignments.

821

822 Figure 7. Schindler diagrams illustrating the charge properties of goethite and ionic SRFA  
823 and DFOB. The horizontal bar in the bottom rectangle indicates the pH range over which  
824 purely electrostatic adsorption mechanisms are possible.

825

826 Figure 8. Proposed adsorption mechanism for the goethite-SRFA complex, involving a  
827 chelate ring incorporating  $\text{COO}^-$  and phenolic OH from SRFA.

828

829 Figure 9. Proposed mechanism of goethite dissolution in the presence of DFOB and SRFA.

830

831

Table 1. Linear regression equations, mass-normalised zero-order dissolution rate coefficients, surface excess values for DFOB, and pseudo-first-order rate coefficients for goethite dissolution at pH 6.5 and 25°C.

System	Regression equation	Rate coefficient ( $\mu\text{mol g}^{-1} \text{h}^{-1}$ )	DFOB surface excess ( $\mu\text{mol g}^{-1}$ )	Pseudo-first- order rate coefficient ( $\text{h}^{-1}$ )
1	$Y = 0.180X + 11.90$	$0.257 \pm 0.016$	14.4	0.018
2	$Y = 0.191X + 14.94$	$0.273 \pm 0.009$	19.0	0.014
3	$Y = 0.188X + 10.00$	$0.268 \pm 0.034$	23.3	0.012
4	$Y = 0.255X + 14.66$	$0.364 \pm 0.014$	18.3	0.020
5	$Y = 0.289X + 14.08$	$0.412 \pm 0.000$	26.5	0.016
6	$Y = 0.308X + 29.72$	$0.440 \pm 0.070$	22.8	0.019

Initial DFOB concentration = 270  $\mu\text{M}$

Goethite concentration = 0.7  $\text{g L}^{-1}$

Y = soluble Fe ( $\mu\text{M}$ )

X = time (h)

Table 2. FTIR absorption bands ( $\text{cm}^{-1}$ ) and their assignments for DFOB, synthetic goethite, SRFA and four complexes: Fe-DFOB, Fe-SRFA, DFOB-SRFA and Fe-DFOB-SRFA.

Assignments are based on Cornell and Schwertmann (2003); Edwards et al. (2005); Cozar et al. (2006); Prasad et al. (2006); and Borer et al. (2009). Vibration modes are designated as follows:  $\nu$ , stretching;  $\delta$ , deformation; s, symmetrical; as, asymmetric.

Assignment	DFOB	Goethite	SRFA	Fe-DFOB	Fe-SRFA	DFOB-SRFA	Fe-DFOB-SRFA
$\nu_{\text{C=O}}$ amide I	1624			1622		1624	
$\nu_{\text{C=O}}$ hydroxamate	1599						
$\nu_{\text{C=N}}$ hydroxamate (resonance)				1568			
$\delta_{\text{N-H}}, \nu_{\text{C-N}}$ amide II	1537						
$\delta_{\text{NOH}}, \nu_{\text{C-N}}, \nu_{\text{C-N}}$ hydroxamate X2, adjacent to hydroxamate	1480						
$\nu_{\text{Fe-O}}$ hydroxamate-iron				1459			
$\nu_{\text{C-N}}, \delta_{\text{C-H}}, \delta_{\text{N-H}}$ hydroxamate X2, terminal N	1386						
$\nu_{\text{N-O}}$ hydroxamate (resonance)	1047			1045		1046	1042
$\nu_{\text{Fe-O}}$ hydroxamate-iron				561			542
$\nu_{\text{OH}}$ (phenolic)			3425		3410	3417	3437
$\nu_{\text{N-H}}$ (terminal N)	3128 3325			3368		2939	3010 2954
$\nu_{\text{C=O}}$ carboxylic acid protonated			1720		1687	1719	1723
$\nu_{\text{as C=O}}$ carboxylic acid deprotonated			1629		1631	1626	1642
$\nu_{\text{s C=O}}$ carboxylic acid deprotonated			1384		1384	1385	
$\nu_{\text{OH}}$ phenolic			1218			1218	1216
$\nu_{\text{(OH)}}$ hydroxyl stretch		3132					
$\delta_{\text{OH}}$ in-plane-hydroxyl		891					
$\delta_{\text{OH}}$ out-of-plane hydroxyl		795					
$\nu_{\text{FeO6}}$ lattice mode		640					

Figure 1  
[Click here to download high resolution image](#)

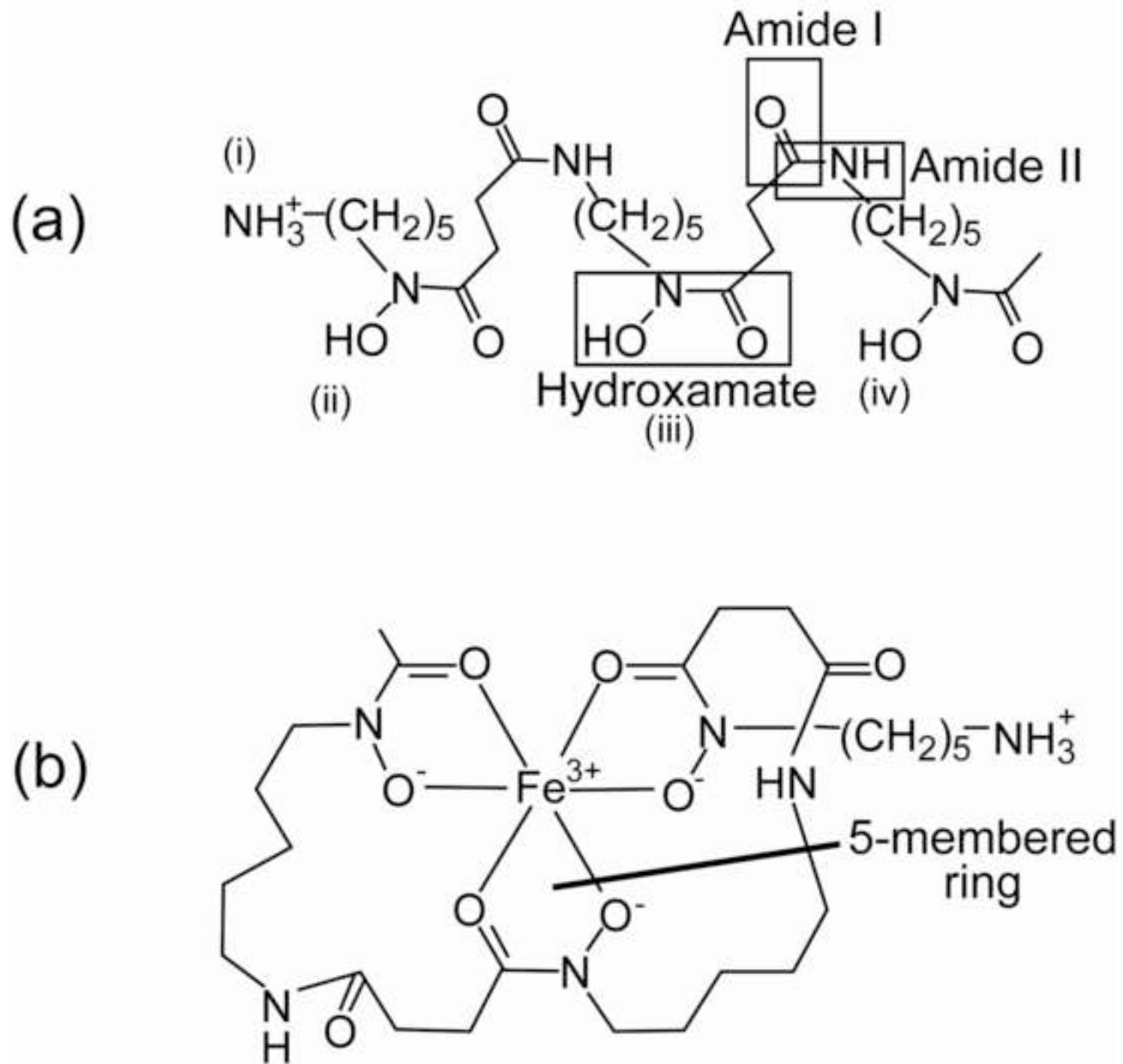
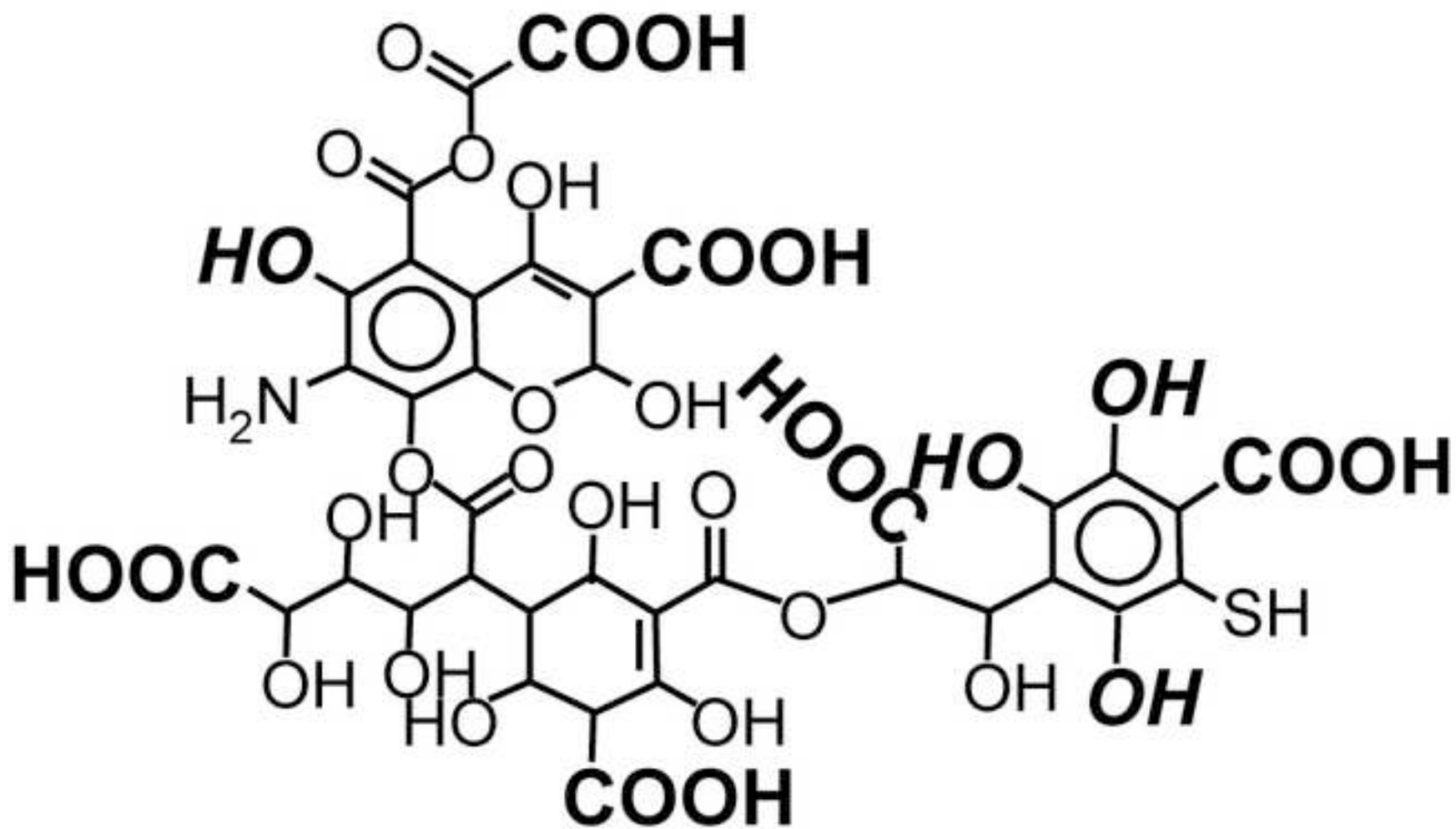


Figure 2

[Click here to download high resolution image](#)



Phenolic group:  $(C_6H_5)OH$ ,  $HO(H_5C_6)$

Carboxylic acid group: **COOH**, **HOOC**

Figure 3  
[Click here to download high resolution image](#)

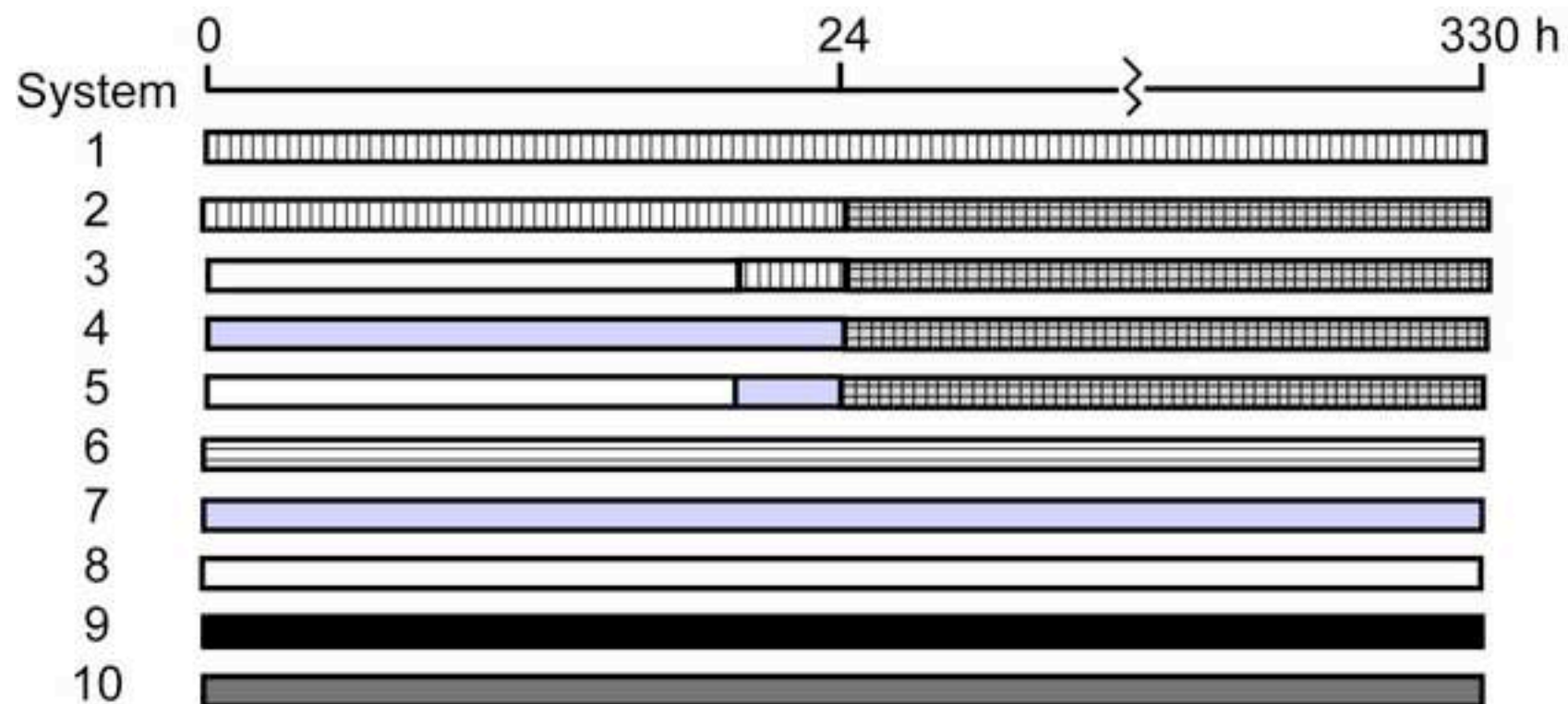


Figure 4  
[Click here to download high resolution image](#)

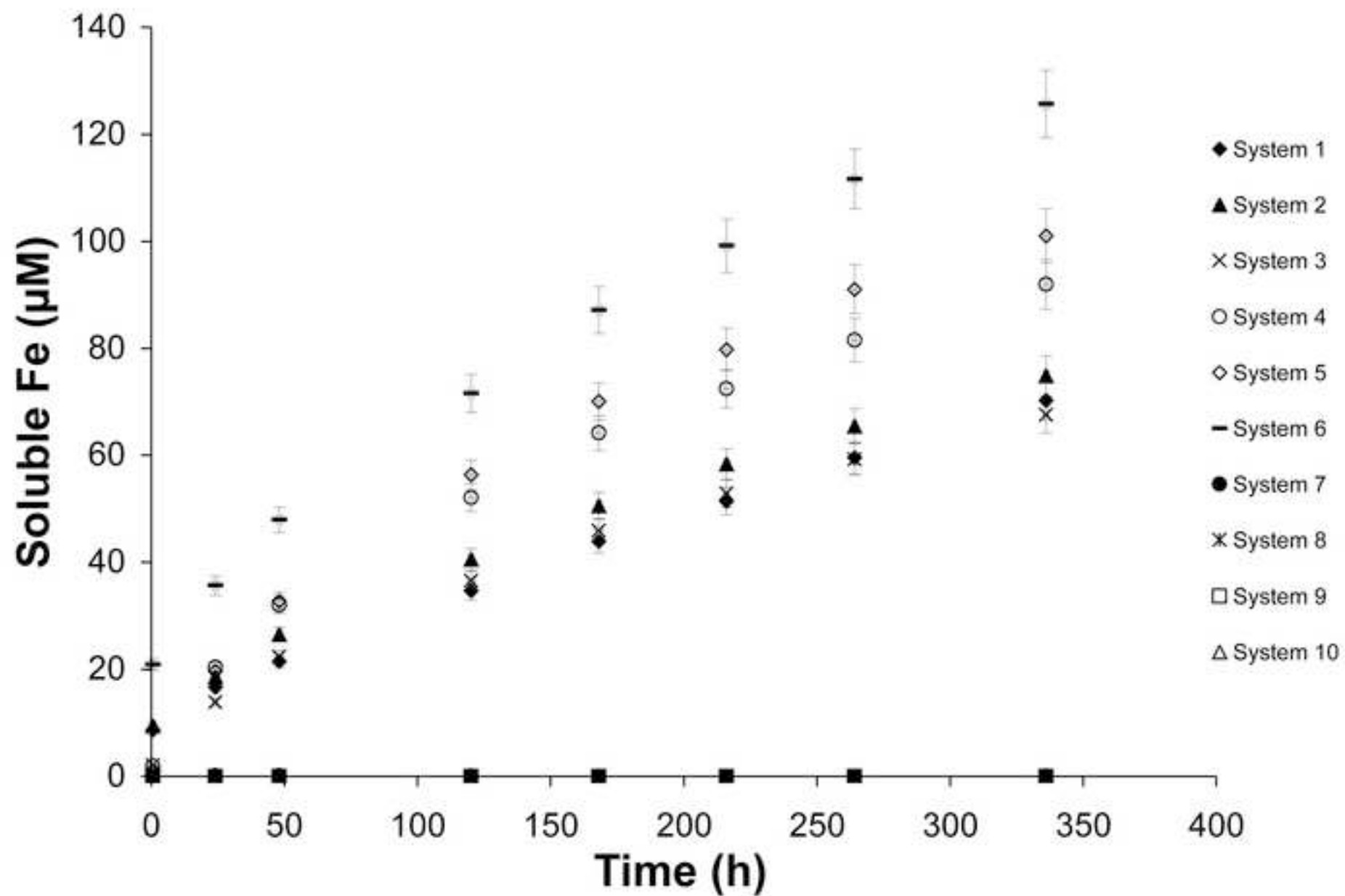




Figure 5  
[Click here to download high resolution image](#)

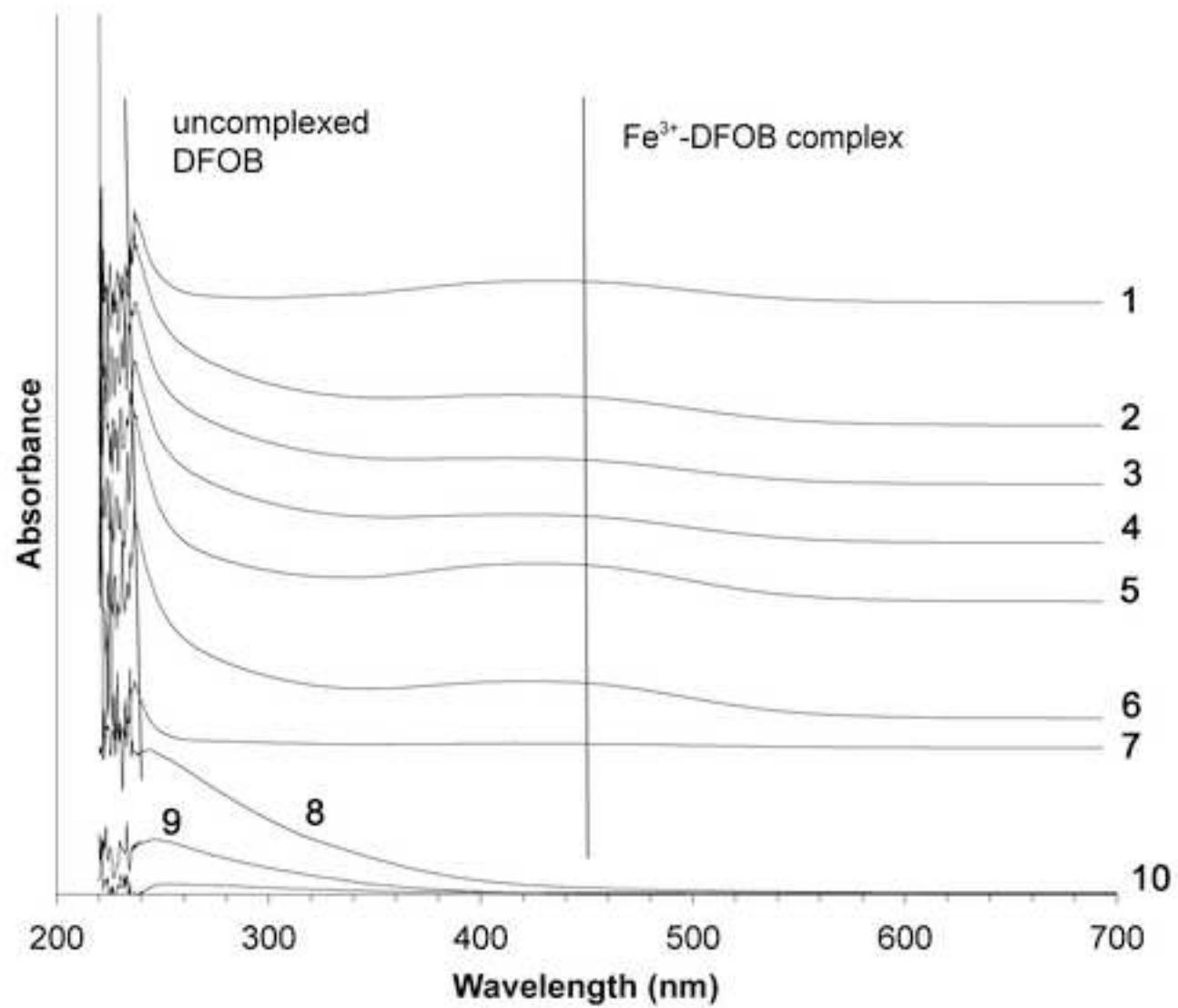


Figure 6  
[Click here to download high resolution image](#)

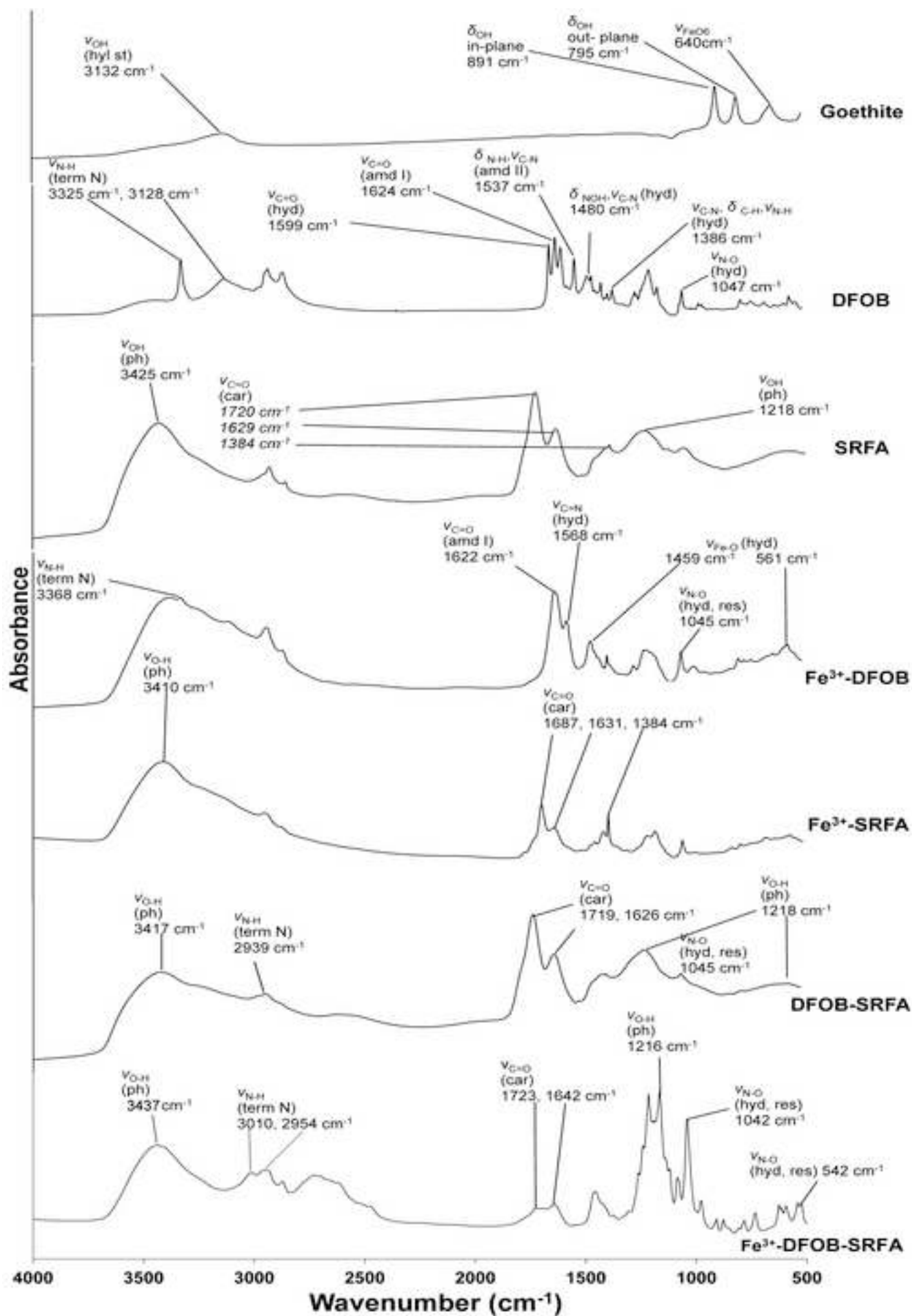


Figure 7  
[Click here to download high resolution image](#)

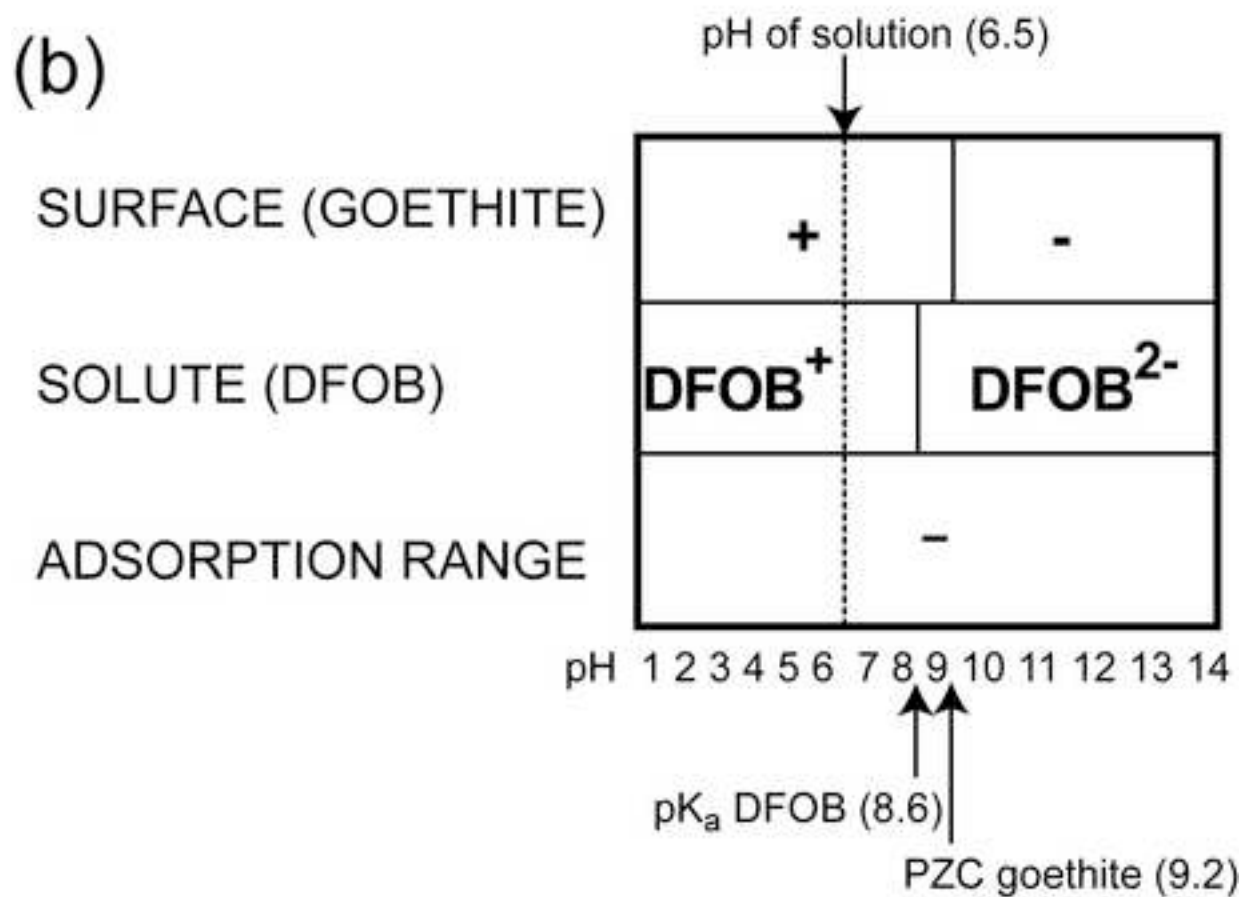
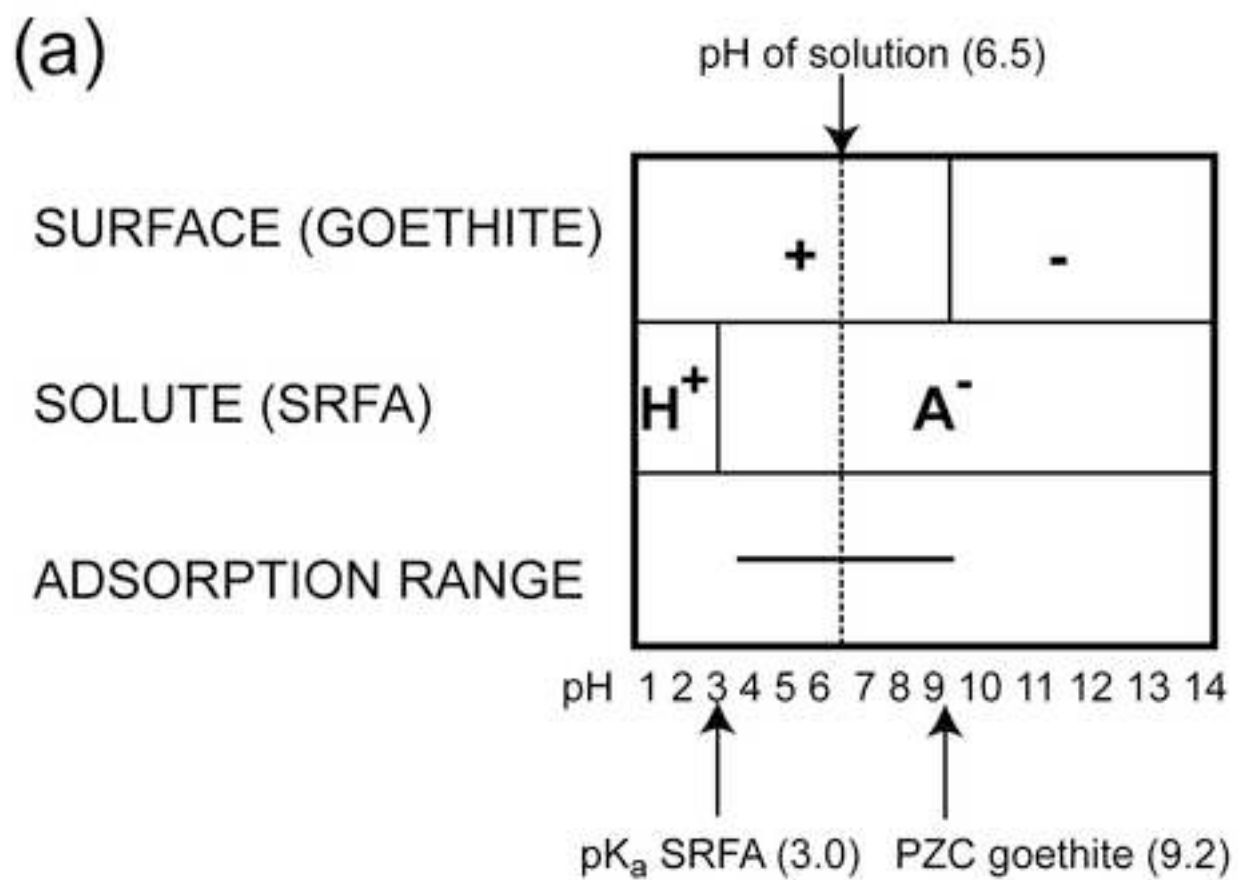
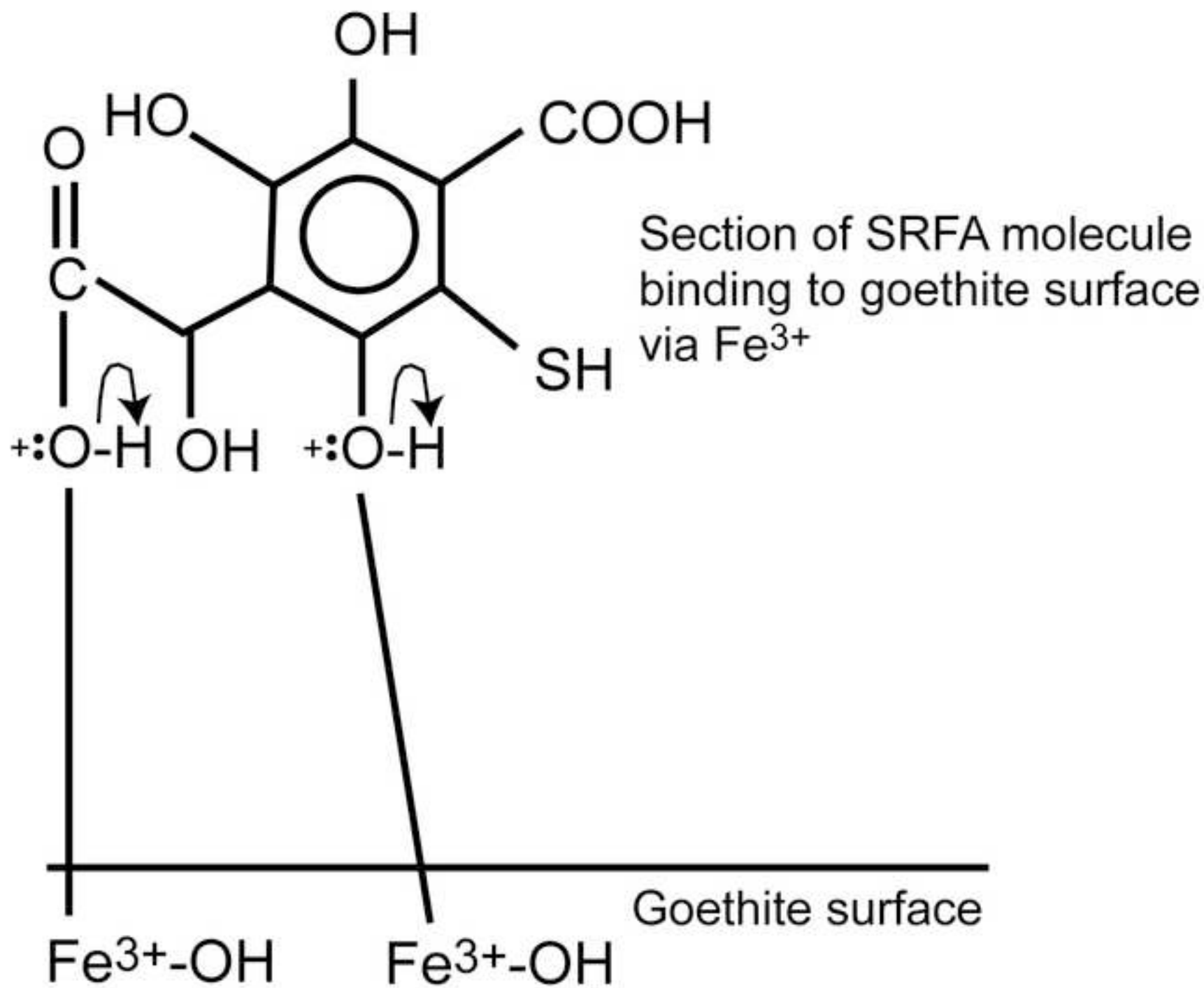
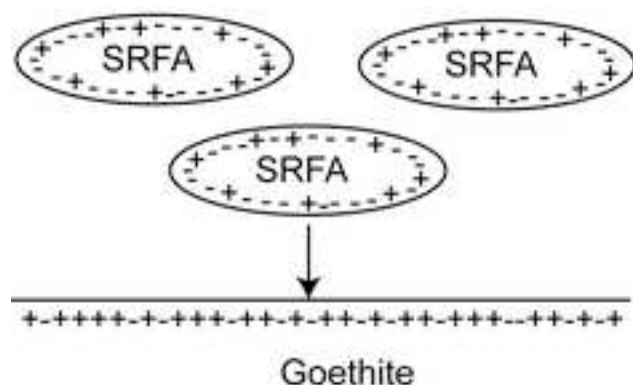


Figure 8

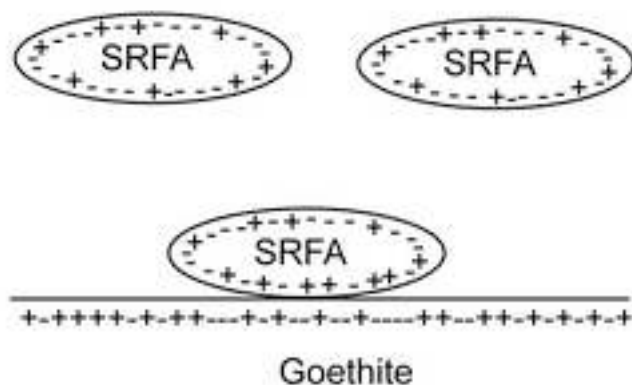
[Click here to download high resolution image](#)



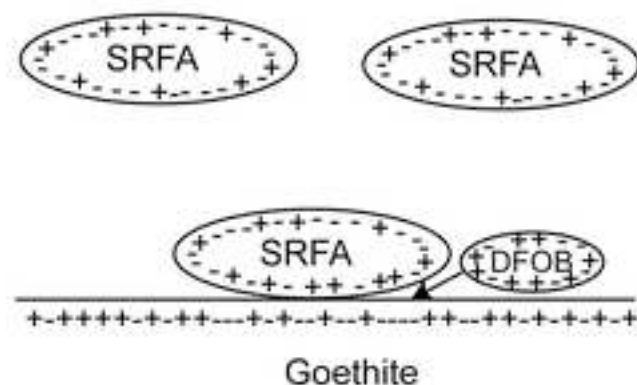
**Figure 9**  
[Click here to download high resolution image](#)



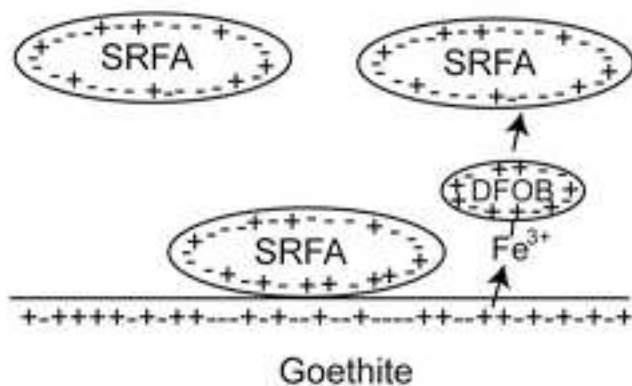
Step 1. At pH 6.5, SRFA surface is negatively charged, and goethite surface is positively charged.



Step 2. Areas on the goethite surface become less positive in the vicinity of the SRFA molecule.



Step 3. The hydroxamate furthest from the protonated amine in the DFOB bonds to the less positive areas on the goethite surface.



Step 4. DFOB bonds with Fe<sup>3+</sup> on the goethite surface. The new Fe<sup>3+</sup>-DFOB complex then detaches from the surface into solution and approaches other SRFA molecules.